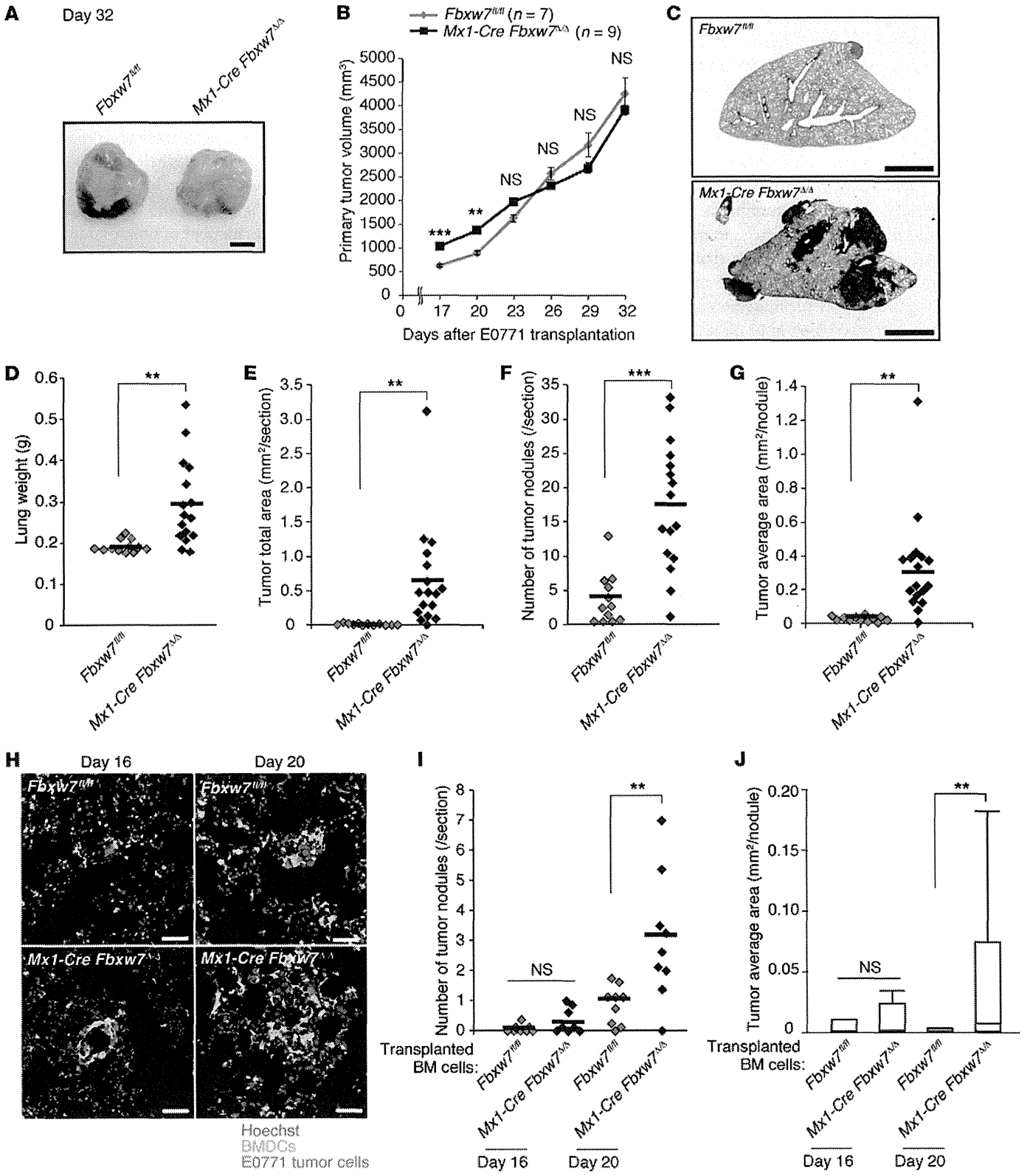

Figure 2. *Fbxw7* deletion in BM promotes cancer metastasis in an orthotopic breast cancer transplantation model. (**A** and **B**) E0771 cells were transplanted into the mammary fat pad of *Fbxw7*$^{fl/fl}$ (n = 11) and *Mx1-Cre Fbxw7*$^{\Delta/\Delta}$ (n = 13) mice. Primary tumor gross appearance after 32 days (**A**) and volume at the indicated times (**B**) are shown. (**C**–**G**) E0771 cells were transplanted into the mammary fat pad of *Fbxw7*$^{fl/fl}$ (n = 12) and *Mx1-Cre Fbxw7*$^{\Delta/\Delta}$ (n = 16) mice. After 32 days, lungs were subjected to H&E staining (**C**), and their gross weight was determined (**D**). Tumor total area (**E**), number of tumor nodules (**F**), and average tumor area (**G**) were calculated from the stained lung sections. (**H**–**J**) WT mice were reconstituted with BM cells of the indicated mice and subjected to orthotopic transplantation with tdTomato-labeled E0771 cells. Lungs were subjected to fluorescence microscopy for detection of BMDCs (green), tumor cells (red), and cell nuclei (Hoechst 33238) (**H**), and the number of tumor nodules (**I**) and average tumor area (**J**) were determined 16 (n = 8 per group) or 20 (n = 9 per group) days after tumor cell transplantation. Scale bars: 2 mm (**C**); 100 μm (**H**). Data in **B** are mean ± SEM; horizontal bars in **D**–**G** and **I** indicate means; box and whisker plots in **J** depict the smallest value, lower quartile, median, upper quartile, and largest value. $^{**}P < 0.01$, $^{***}P < 0.001$, 2-tailed Student's t test (**B**, **D**–**G**, **I**, and **J**).

resent increased migration or recruitment of Mo-MDSCs and macrophages, rather than differentiation of these cells in BM.

Serum chemokine levels are increased in mice lacking FBXW7 in BM. To explore the mechanism responsible for this increased mobilization of Mo-MDSCs and macrophages induced by FBXW7 deficiency, we examined the serum concentrations of various cytokines before and after E0771 cell transplantation. Cytokine array analysis revealed that the levels of CCL2, CCL12 (also known as MCP-5), and the chemokine CXCL13 (also known as B lymphocyte chemoattractant [BLC]) were increased more than 2-fold in *Mx1-Cre Fbxw7*$^{\Delta/\Delta}$ versus control mice both before and after E0771 cell transplantation (Figure 4A and Supplemental Figure 4). Both CCL2 and CCL12 induce the migration of monocytes/macrophages by binding to their common receptor, CCR2. CCL12 is mainly secreted from macrophages, but *Fbxw7* ablation in the macrophages of *LysM-Cre Fbxw7*$^{fl/fl}$ mice did not affect metastasis frequency (Supplemental Figure 5, A and B), which suggests that CCL12 is not largely responsible for the promotion of metastasis. We thus focused on CCL2 and found greater serum CCL2 concentrations in *Mx1-Cre Fbxw7*$^{\Delta/\Delta}$ mice compared with control mice both before and after E0771 cell transplantation (Figure 4B).

To examine whether the enhanced metastasis apparent in FBXW7-deficient mice is dependent on the CCL2/CCR2 pathway, we treated *Mx1-Cre Fbxw7*$^{\Delta/\Delta}$ mice with propagermanium, a CCR2 antagonist. The extent of B16F10 or E0771 cell metastasis in *Mx1-Cre Fbxw7*$^{\Delta/\Delta}$ mice was significantly attenuated by propagermanium administration (Figure 4, C–H). The frequency of EGFP$^+$Ly6C$^+$ cells in the lungs of WT mice reconstituted with EGFP-labeled *Mx1-Cre Fbxw7*$^{\Delta/\Delta}$ BM cells and injected with E0771 cells was also significantly reduced by propagermanium treatment (Figure 4H). Unexpectedly, the number of tumor nodules in the lungs was not affected by propagermanium treatment, whereas the size of each nodule was markedly reduced in the treated mice (Figure 4, F and G). Collectively, these results suggested that the increased production of CCL2 by FBXW7-deficient BMDCs promotes the growth of tumors that have already metastasized to the lungs.

The Ccl2 gene is activated in FBXW7-deficient BMSCs. We next investigated which cells of the BM are responsible for the metastasis promotion and increased serum CCL2 concentration observed in FBXW7-deficient mice. For these experiments, we used mice deficient in FBXW7 in different lineages. *LysM-Cre Fbxw7*$^{-/\Delta}$ mice, in which the *Cre* gene is activated to delete floxed *Fbxw7* alleles only in the granulocyte-macrophage lineage, did not show an increase in metastasis frequency compared with control mice (Supplemental Figure 5, A and B). Furthermore, neither *Lck-Cre Fbxw7*$^{\Delta/\Delta}$ nor *Cd19-Cre Fbxw7*$^{\Delta/\Delta}$ mice (*Fbxw7* deletion specific to T and B cells, respectively) showed enhancement of metastasis like that in *Mx1-Cre Fbxw7*$^{\Delta/\Delta}$ mice (Supplemental Figure 5, C–F). These results suggested that neither myeloid (granulocyte and macrophage) nor lymphoid (T and B cell) lineages are responsible for the promotion of metastasis induced by BM *Fbxw7* ablation.

Neither the serum level of CCL2 nor the frequency of MAC1$^+$F4/80$^+$ monocytes/macrophages in peripheral blood differed between *LysM-Cre Fbxw7*$^{-/\Delta}$ and control mice (Supplemental Figure 6, A and B), which suggests that monocytes/macrophages are not the major source of CCL2 produced in response to *Fbxw7* loss. We found that FSP$^+$ BMSCs colocalized with metastatic tumor cells and Mo-MDSCs in the lungs of mice after orthotopic transplantation of E0771 cells (Figure 5A). Given that BMSCs were previously shown to secrete CCL2 and to contribute to the emigration of monocytes from BM (45, 46), we hypothesized that BMSCs might be a major source of CCL2 production in our models. To test this hypothesis, we isolated BMSCs from BM of *CAG-Cre-ER*^{T2} *Fbxw7*$^{fl/fl}$ (or control *Fbxw7*$^{fl/fl}$) mice and treated them with 10 μM tamoxifen to induce deletion of floxed *Fbxw7* alleles (Figure 5B). The abundance of *Ccl2* mRNA was increased in *CAG-Cre-ER*^{T2} *Fbxw7*$^{\Delta/\Delta}$ BMSCs compared with control cells (Figure 5C). The amount of CCL2 released from *CAG-Cre-ER*^{T2} *Fbxw7*$^{\Delta/\Delta}$ BMSCs into the culture medium was also substantially greater than that released from control cells (Figure 5D). Furthermore, the introduction of WT *Fbxw7a* cDNA into *CAG-Cre-ER*^{T2} *Fbxw7*$^{\Delta/\Delta}$ BMSCs resulted in a marked decrease in the abundance of *Ccl2* mRNA, whereas introduction of cDNA for a mutant form of *Fbxw7a* that lacks the F-box domain (ΔF) had no such effect (Figure 5E), which suggests that FBXW7 negatively regulates CCL2 production in BMSCs.

To examine whether the increased CCL2 production by BMSCs is responsible for the promotion of cancer metastasis in FBXW7-deficient mice, we depleted *CAG-Cre-ER*^{T2} *Fbxw7*$^{\Delta/\Delta}$ BMSCs of CCL2 by shRNA-mediated RNAi (Figure 5F) and then transferred these cells, together with B16F10 melanoma cells, into recipient mice via the tail vein. BMSCs were detected in many tissues, such as BM and lungs, even 4 months after transplantation (47). The extent of lung metastasis in recipient mice was increased by *Fbxw7*$^{\Delta/\Delta}$ versus control BMSCs when coinjected with melanoma cells (Figure 5, G and H). However, this effect of *Fbxw7* deletion was abolished by depletion of CCL2 in BMSCs, which suggests that the increased production of CCL2 by FBXW7-deficient BMSCs contributes to the promotion of metastasis.

NOTCH accumulation in FBXW7-deficient BMSCs promotes metastasis by increasing CCL2 production. Immunoblot analysis revealed that, among the FBXW7 substrates examined, NOTCH1 intracellular domain (NICD1), c-MYC, and KLF5 accumulated at high levels in FBXW7-deficient BMSCs (Figure 6A). Forced expression of NICD1 in WT BMSCs resulted in a marked increase both in the abundance of *Ccl2* mRNA and in the activity of the *Ccl2* gene promoter, whereas that of c-MYC or KLF5 had no such effects (Figure 6, B and C). Inhibition of NOTCH signaling in FBXW7-deficient BMSCs by exposure to the γ-secretase inhibitor *N*-[*N*-(3,5-difluorophenacetyl)-L-alanyl]-*S*-phenylglycine *t*-butyl ester (DAPT) resulted in a concentration-dependent reduction in the amount of *Ccl2* mRNA (Figure 6D). The promoter of the mouse *Ccl2* gene contains 4 consensus sequences for NOTCH binding (Figure 6E and ref. 48), and a luciferase reporter assay with WT and mutant forms of this promoter indicated that the first 2 upstream elements are required for full promoter activity (Figure 6F). This finding was consistent with the results of ChIP analysis showing that NICD1 was associated with the distal region of the *Ccl2* gene promoter in *Fbxw7*$^{\Delta/\Delta}$ BMSCs (Figure 6G). Together, these observations suggested that the NOTCH/CCL2 pathway in BMSCs contributes to the promotion of metastasis in FBXW7-deficient mice.

We further evaluated this notion by genetic analyses. Additional ablation of RBP-Jκ, an essential cofactor for NOTCH-dependent transactivation, markedly attenuated the enhanced metastasis observed in *Mx1-Cre Fbxw7*$^{\Delta/\Delta}$ mice (Figure 6, H and I).

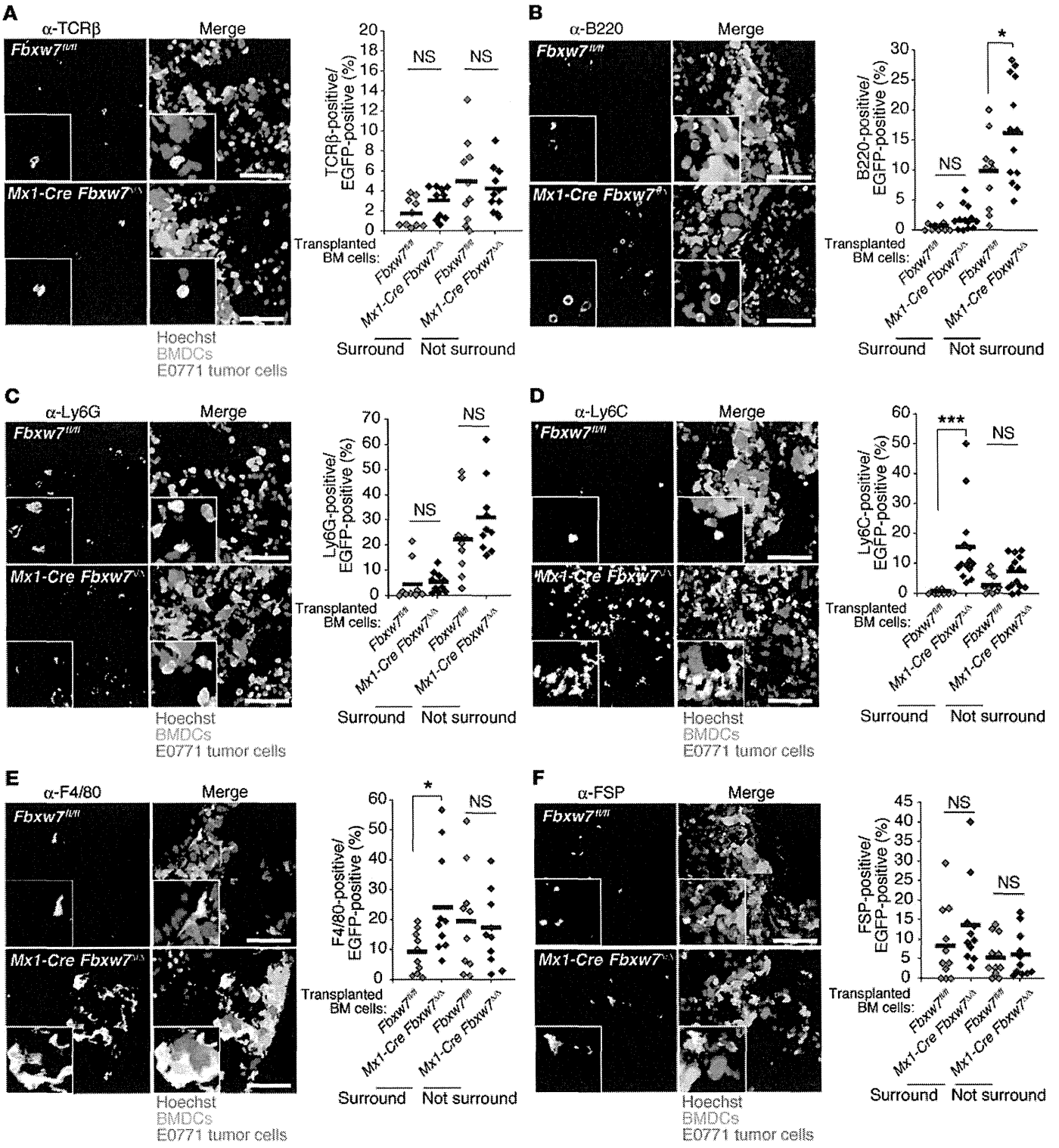

Figure 3. Ly6C⁺ Mo-MDSCs and F4/80⁺ monocytes/macrophages accumulate in the microenvironment of metastatic tumors in the lungs of mice reconstituted with FBXW7-deficient BM cells. Representative immunohistofluorescence staining (white) for TCRβ (**A**), B220 (**B**), Ly6G (**C**), Ly6C (**D**), F4/80 (**E**), and FSP (**F**) for lung sections from WT mice reconstituted with *CAG-EGFP Fbxw7*$^{fl/fl}$ (n = 10 [**A**, **B**, **D**, and **E**]; 9 [**C**]; 11 [**F**]) or *CAG-EGFP Mx1-Cre Fbxw7*$^{\Delta/\Delta}$ (n = 10 [**A**, **C**, and **E**]; 12 [**B**]; 14 [**D**]; 11 [**F**]) BM cells and subjected to orthotopic transplantation with tdTomato-labeled E0771 cells (20 days before analysis) as in Figure 2H. Intrinsic fluorescence of EGFP (green), tdTomato (red), and Hoechst 33258 (blue) was also imaged. Higher-magnification images (×2) are shown in the insets. Scale bars: 100 μm. The percentage of EGFP⁺ BMDCs positive for each marker in tumor-surrounding and nonsurrounding regions was quantified; horizontal bars indicate means. $^*P < 0.05$, $^{***}P < 0.001$, 1-way ANOVA and Bonferroni test.

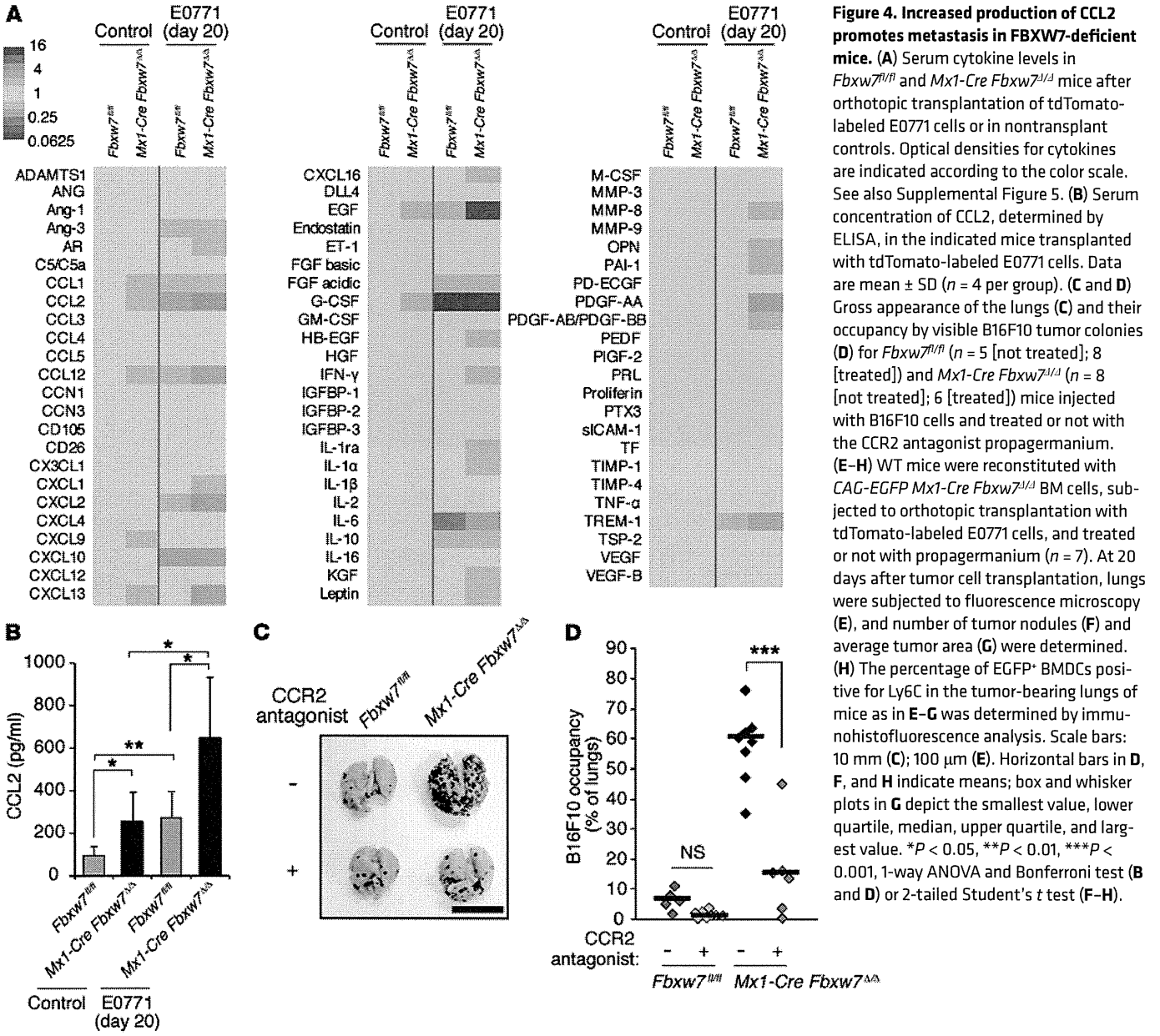

Figure 4. Increased production of CCL2 promotes metastasis in FBXW7-deficient mice. (**A**) Serum cytokine levels in *Fbxw7*$^{fl/fl}$ and *Mx1-Cre Fbxw7*$^{\Delta/\Delta}$ mice after orthotopic transplantation of tdTomato-labeled E0771 cells or in nontransplant controls. Optical densities for cytokines are indicated according to the color scale. See also Supplemental Figure 5. (**B**) Serum concentration of CCL2, determined by ELISA, in the indicated mice transplanted with tdTomato-labeled E0771 cells. Data are mean ± SD (n = 4 per group). (**C** and **D**) Gross appearance of the lungs (**C**) and their occupancy by visible B16F10 tumor colonies (**D**) for *Fbxw7*$^{fl/fl}$ (n = 5 [not treated]; 8 [treated]) and *Mx1-Cre Fbxw7*$^{\Delta/\Delta}$ (n = 8 [not treated]; 6 [treated]) mice injected with B16F10 cells and treated or not with the CCR2 antagonist propagermanium. (**E**–**H**) WT mice were reconstituted with *CAG-EGFP Mx1-Cre Fbxw7*$^{\Delta/\Delta}$ BM cells, subjected to orthotopic transplantation with tdTomato-labeled E0771 cells, and treated or not with propagermanium (n = 7). At 20 days after tumor cell transplantation, lungs were subjected to fluorescence microscopy (**E**), and number of tumor nodules (**F**) and average tumor area (**G**) were determined. (**H**) The percentage of EGFP$^+$ BMDCs positive for Ly6C in the tumor-bearing lungs of mice as in **E**–**G** was determined by immunohistofluorescence analysis. Scale bars: 10 mm (**C**); 100 μm (**E**). Horizontal bars in **D**, **F**, and **H** indicate means; box and whisker plots in **G** depict the smallest value, lower quartile, median, upper quartile, and largest value. *P < 0.05, **P < 0.01, ***P < 0.001, 1-way ANOVA and Bonferroni test (**B** and **D**) or 2-tailed Student's t test (**F**–**H**).

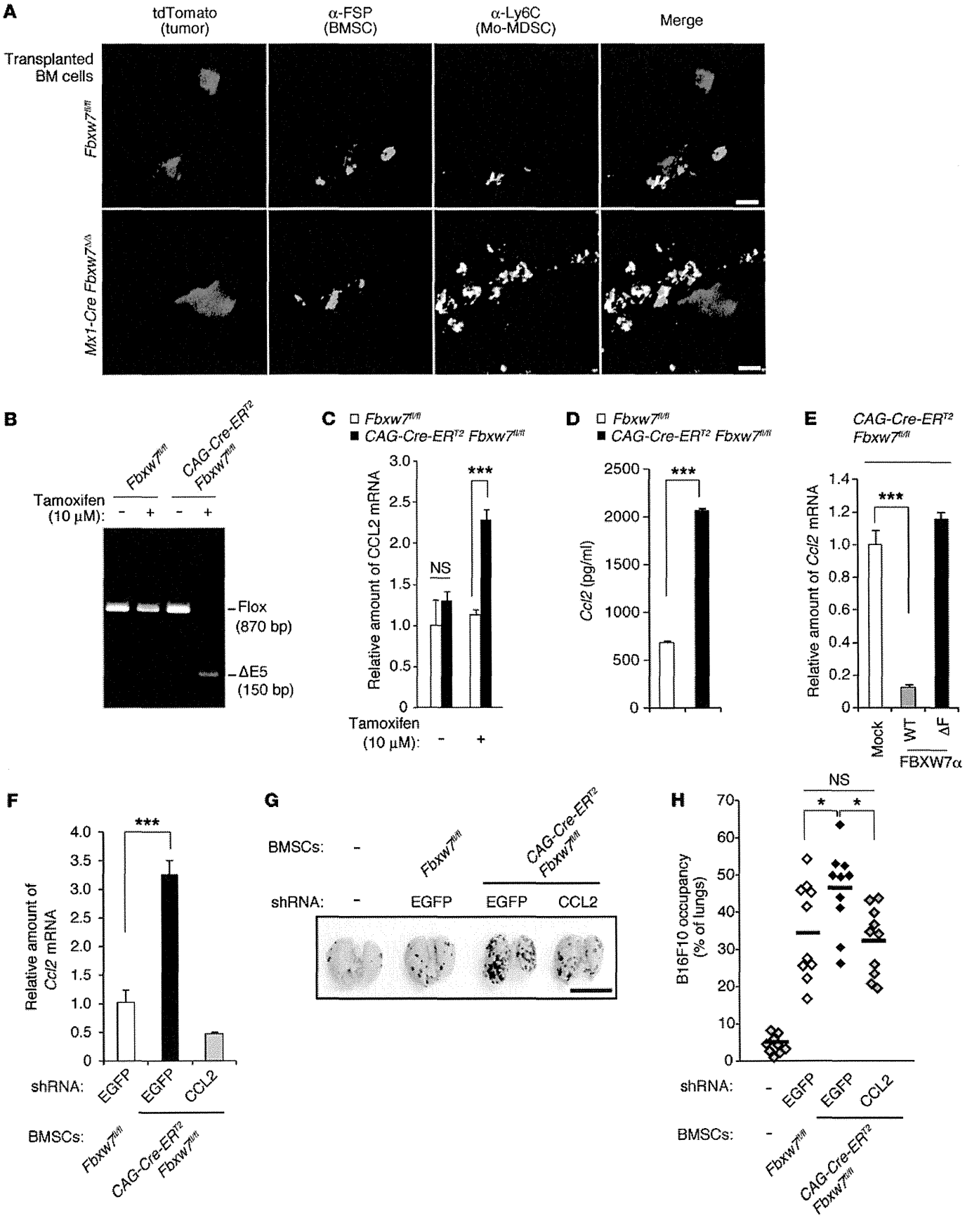

Figure 5. Increased *Ccl2* gene expression in FBXW7-deficient BMSCs promotes cancer metastasis. (**A**) Representative immunohistofluorescence staining of Ly6C and FSP in lung sections from WT mice reconstituted with indicated BM cells and subjected to orthotopic transplantation with tdTomato-labeled E0771 cells (20 days before analysis). (**B**) Genomic PCR analysis of BMSCs from the indicated mice incubated in the absence or presence of 10 μM tamoxifen. The positions of amplified fragments corresponding to floxed and exon 5–deleted (Δ5) *Fbxw7* alleles are indicated. (**C**) Relative abundance of *Ccl2* mRNA in BMSCs from the indicated mice. (**D**) Concentration of CCL2 released into culture supernatants from the indicated BMSCs. (**E**) Relative abundance of *Ccl2* mRNA in *CAG-Cre-ER*^{TZ} *Fbxw7*$^{\Delta/\Delta}$ BMSCs infected with retroviruses encoding WT or ΔF mutant forms of FBXW7α or with the empty virus (Mock). (**F**) Relative abundance of *Ccl2* mRNA in BMSCs from *Fbxw7*$^{fl/fl}$ or *CAG-Cre-ER*^{TZ} *Fbxw7*$^{fl/fl}$ mice treated with tamoxifen and subjected to RNAi with shRNA vectors targeting EGFP (control) or CCL2. (**G** and **H**) Gross appearance of the lungs (**G**) and their occupancy by visible B16F10 colonies (**H**) for WT mice 2 weeks after injection both with B16F10 cells and with BMSCs isolated from the indicated mice and treated as in **F** (n = 10 per group). Scale bars: 10 μm (**A**), 10 mm (**G**). Data are mean ± SD (**C**–**F**); horizontal bars in **H** indicate means. *$P < 0.05$, ***$P < 0.001$, 1-way ANOVA and Bonferroni test (**C**, **E**, **F**, and **H**) or 2-tailed Student's t test (**D**).

In contrast, inactivation of c-MYC in *Mx1-Cre Fbxw7*$^{\Delta/\Delta}$ mice had no such effect (Figure 6, J and K). Additional ablation of RBP-Jκ, but not that of c-MYC, also reduced the serum concentration of CCL2 to the control level in *Mx1-Cre Fbxw7*$^{\Delta/\Delta}$ mice (Figure 6L).

Low FBXW7 expression in the host microenvironment is associated with poor prognosis in breast cancer patients. To extend our observations in mice to humans, we measured the abundance of *FBXW7* mRNA in peripheral blood of breast cancer specimens and examined the relationship between *FBXW7* mRNA abundance and prognosis. The prognosis of individuals with low *FBXW7* expression in peripheral blood was significantly poorer than that of those in the corresponding high-*FBXW7* group (Figure 7, A and B), consistent with our model. The difference in prognosis between the low- and high-expression groups was even more pronounced when the analysis was restricted to patients with tumors triple-negative for estrogen receptor (ER), progesterone receptor (PR), and HER2 (Figure 7, C–E) or to those with tumors of high histological grade or low stage (Supplemental Figure 7, A–G). The frequency of CD45$^-$ circulating tumor cells that expressed CD326 (also known as EpCAM) was at most 0.003% of total blood mononuclear cells (Supplemental Figure 7H), which suggests that the contribution of such cells to the total abundance of *FBXW7* mRNA in peripheral blood is negligible.

Immunohistochemical analysis of FBXW7 in primary tumor lesions revealed that the abundance of *FBXW7* mRNA in peripheral blood was not significantly correlated with FBXW7 expression in tumor cells, but was highly correlated with that in surrounding stromal cells (Figure 7, F–H). These results suggested that the abundance of *FBXW7* mRNA in peripheral blood is a marker for FBXW7 expression in stromal cells that surround tumor cells. We also observed a negative correlation between *FBXW7* mRNA abundance in peripheral blood and serum CCL2 concentration (Figure 7I). High serum levels of CCL2 were associated with poor prognosis in breast cancer patients (S. Akiyoshi and K. Mimori, unpublished observation). These data support our concept that FBXW7 ablation gives rise to increased CCL2 production, facilitating metastatic tumor growth (Figure 8).

Discussion

The *FBXW7* gene is a potent tumor suppressor, as evidenced by the many corresponding mutations associated with human cancer (37) as well as by the tumor formation observed in conditional knockout mice (38, 39, 41). The anticancer function of FBXW7 is thought to be mediated by specific ubiquitylation both of growth-promoting oncoproteins — such as c-MYC (24, 25), NOTCH (26, 27, 49), cyclin E (29–31), c-JUN (32, 33), KLF5 (34, 35), and mTOR (36) — and of the antiapoptotic molecule MCL-1 (50, 51). Most previous studies have focused on the tumor-suppressive role of FBXW7 in tumor cells themselves. The putative tumor suppressor C/EBPδ was shown to inhibit FBXW7 expression and to promote mammary tumor metastasis through attenuation of FBXW7-dependent degradation of mTOR in tumor cells (52). We have now discovered what we believe to be a new aspect of FBXW7 function in tumor suppression — namely, its role in the host environment to suppress cancer metastasis. Our data also provide mechanistic insight into the suppression of cancer metastasis by FBXW7. We found that NOTCH, one of the major substrates of FBXW7, activated transcription of the gene encoding CCL2, one of the most well-characterized chemokines with respect to cancer development. Our human clinical data, showing that reduced *FBXW7* expression in peripheral blood was associated with a poor prognosis in breast cancer patients, appeared to be consistent with our experimental results in mice. We therefore propose that the FBXW7/NOTCH/CCL2 axis in the host environment limits cancer metastasis.

CCL2 is thought to be secreted from both cancer cells and noncancer cells in the tumor environment. In a xenograft model in which human cancer cells were transplanted into mice, administration of antibodies specific for human or mouse CCL2 inhibited tumor growth and metastasis, which supports the notion that CCL2 secreted from both the tumor and the host environment plays a key role in tumor development (19, 21). It is likely that the FBXW7/NOTCH1/CCL2 axis in cancer cells also plays a key role in metastasis. We showed here that the level of *FBXW7* expression in peripheral blood was related to prognosis in breast cancer patients. These results thus suggest that constitutional variability in *FBXW7* expression might be an important determinant of prognosis. We propose that the level of *FBXW7* expression is a potentially powerful prognostic marker for cancer patients in general, and that targeting the CCL2/CCR2 system might prove a rational approach for preventing cancer metastasis. Indeed, we found that the CCR2 antagonist propagermanium had a marked inhibitory effect on cancer metastasis in mice. Propagermanium is currently administered clinically for the treatment of individuals with hepatitis B virus infection, and its long-term safety has been well demonstrated. Our results suggest that evaluation of this drug for its ability to inhibit cancer metastasis in humans is warranted.

We found that the number of tumor nodules in the lungs and the average area per nodule were greater in FBXW7-deficient mice than in controls subjected to orthotopic transplantation of breast cancer cells. Unexpectedly, however, treatment with propagermanium did not affect the number of tumor nodules, although the size of each nodule and the frequency of associated Mo-MDSCs were markedly reduced. Collectively, these results suggest that CCL2-dependent infiltration of Mo-MDSCs in the lungs influences the growth of established metastatic tumors rather than the

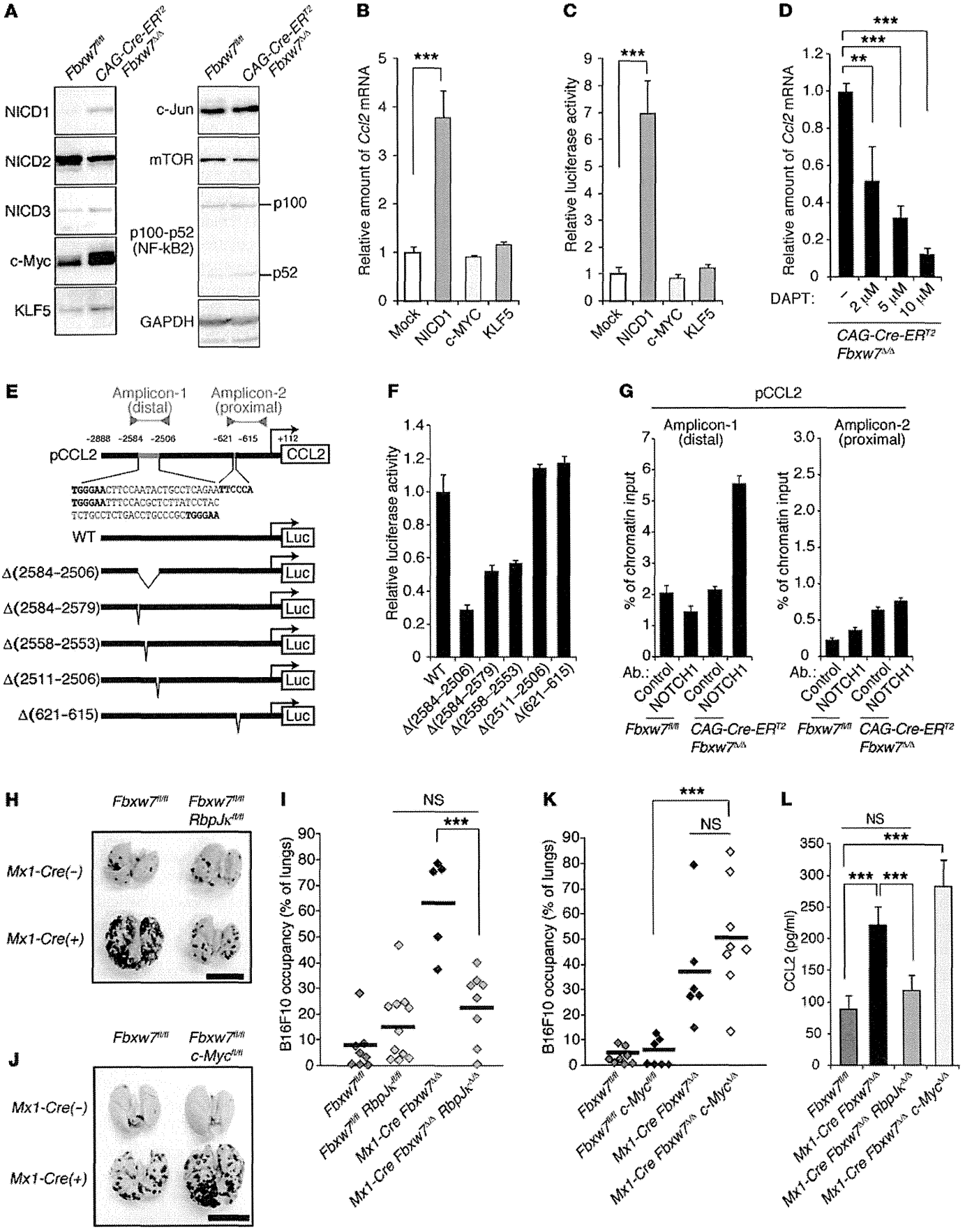

Figure 6. NOTCH accumulation in FBXW7-deficient BMSCs promotes CCL2 expression and cancer metastasis. (**A**) Immunoblot analysis of FBXW7 substrates in the indicated BMSCs. (**B**) Relative abundance of *Ccl2* mRNA in WT BMSCs infected with retroviruses encoding NICD1, c-MYC, or KLF5. (**C**) Luciferase assay for the *Ccl2* gene in BMSCs infected with retroviruses for NICD1, c-MYC, or KLF5. (**D**) Relative abundance of *Ccl2* mRNA in *CAG-Cre-ER^{T2} Fbxw7$^{\Delta/\Delta}$* BMSCs incubated with DAPT. (**E**) WT and mutant forms of the mouse *Ccl2* gene promoter fused to the firefly luciferase gene. Consensus binding sequences for NOTCH–RBP-Jκ are shown in bold. Proximal and distal amplicons in **G** are indicated. (**F**) Luciferase assay for the *Ccl2* gene in *CAG-Cre-ER^{T2} Fbxw7$^{\Delta/\Delta}$* BMSCs. (**G**) ChIP analysis of the *Ccl2* gene promoter. Immunoprecipitation was performed with antibodies against NOTCH1 or with control IgG. (**H** and **I**) Intravenous transplantation with B16F10 cells for *Fbxw7$^{fl/fl}$* (n = 8), *Fbxw7$^{fl/fl}$ Rbpjκ$^{fl/fl}$* (n = 11), *Mx1-Cre Fbxw7$^{\Delta/\Delta}$* (n = 5), and *Mx1-Cre Fbxw7$^{\Delta/\Delta}$ Rbpjκ$^{\Delta/\Delta}$* (n = 8) mice. (**J** and **K**) Intravenous transplantation with B16F10 cells for *Fbxw7$^{fl/fl}$* (n = 8), *Fbxw7$^{fl/fl}$ c-Myc$^{fl/fl}$* (n = 7), *Mx1-Cre Fbxw7$^{\Delta/\Delta}$* (n = 6), and *Mx1-Cre Fbxw7$^{\Delta/\Delta}$ c-Myc$^{\Delta/\Delta}$* (n = 8) mice. Gross appearance of the lungs (**H** and **J**) and their occupancy by B16F10 colonies (**I** and **K**) are shown. (**L**) Serum concentration of CCL2, determined by ELISA. Scale bars: 10 mm (**H** and **J**). Data are mean ± SD (n = 3) (**B**–**D**, **F**, **G**, and **L**); horizontal bars in **I** and **K** indicate means. $^{**}P < 0.01$, $^{***}P < 0.001$, 1-way ANOVA and Bonferroni test (**B**–**D**, **I**, **K**, and **L**).

recruitment of tumor cells to the lungs, which might be regulated by other factors, such as CXCL13, triggering receptor expressed on myeloid cells 1 (TREM1); epidermal growth factor, CXCL2 (also known as macrophage inflammatory protein 2α [MIP-2α]); and PDGF-AA. The serum levels of these proteins were increased or decreased more than 2-fold in *Mx1-Cre Fbxw7$^{\Delta/\Delta}$* mice compared with controls after E0771 cell transplantation. Further studies are needed to elucidate the molecular mechanisms responsible for the increase in tumor cell engraftment in FBXW7-deficient mice.

In the present study, infiltration of Mo-MDSCs and macrophages into metastatic tumor lesions was promoted by the increased production of chemokines such as CCL2 in FBXW7-deficient mice. We found that BMSCs likely represent a major source of CCL2 production, although a possible contribution of other BMDCs cannot be excluded. In humans, CCL2 produced from other cell types — such as fibroblasts, endothelial cells, and smooth muscle cells — is also thought to promote cancer metastasis (53–56). Our identification of FBXW7 and NOTCH as upstream regulators of CCL2 expression provides both important insight into the mechanism by which production of this chemokine is regulated and a basis for the development of new strategies for cancer treatment.

Methods

Analysis of human clinical specimens. All clinical results in this study are from retrospective studies. Peripheral blood specimens were obtained from 406 Japanese women with breast cancer who underwent surgery between 2000 and 2005 at the National Kyushu Cancer Center. All patients were clearly identified as having breast cancer based on clinicopathologic findings, and none underwent chemotherapy or radiotherapy before surgery. Collection of peripheral blood through a venous catheter for the measurement of *FBXW7* mRNA was performed immediately before surgery with the patients under general anesthesia. The initial 1.0 ml of peripheral blood was discarded to avoid contamination by skin cells; the second 1.0 ml was mixed with 4.0 ml Isogen-LS (Nippon Gene) for extraction of total RNA.

Mice. Fbxw7$^{fl/fl}$ mice, homozygous for the floxed *Fbxw7* allele (38), were crossed with *Mx1-Cre* transgenic mice (provided by K. Rajewsky, University of Cologne, Cologne, Germany; ref. 57), and deletion of the floxed allele in the resulting offspring was induced by intraperitoneal injection (6 total injections on alternate days) with 20 μg poly(I:C) (Calbiochem) per gram of body weight. Deletion of exon 5 of the floxed *Fbxw7* allele was confirmed by PCR analysis of genomic DNA as previously described (38). *Fbxw7$^{fl/fl}$* mice were also crossed with *Rbpjκ$^{fl/fl}$* mice (provided by T. Honjo, Kyoto University, Kyoto, Japan; ref. 58) or *c-Myc$^{fl/fl}$* mice (provided by I.M. de Alborán, Centro Nacional de Biotecnologia/Consejo Superior de Investigaciones Científicas [CNB/CSIC], Madrid, Spain; ref. 59) or with *Lck-Cre* (60), *LysM-Cre* (61), *Cd19-Cre* (62), *CAG-Cre-ER^{T2}* (63), or *CAG-EGFP* (provided by M. Okabe, Osaka University, Osaka, Japan; ref. 64) transgenic mice.

BM transplantation. C57BL/6 or other recipient mice (8 weeks of age) were irradiated with a lethal dose (11 Gy) of γ rays and injected via the tail vein with BM cells (2.0×10^6 in 100 μl PBS) isolated from 8-week-old *CAG-EGFP*, *CAG-EGFP Fbxw7$^{fl/fl}$*, or *CAG-EGFP Mx1-Cre Fbxw7$^{fl/fl}$* mice. At 2 months after transplantation, recipients were injected with poly(I:C) as described above to delete floxed *Fbxw7* alleles; at 3 days after the final poly(I:C) injection, animals were injected with B16F10, LLC, or E0771 cells as described below. Recipient peripheral blood cells were examined for chimerism by flow cytometry each month after BM transplantation as well as at the time of lung dissection.

Assay of tumor metastasis. Suspensions of B16F10 (2.0×10^5), B16F1 (2.0×10^5), or LLC (5.0×10^5) cells in PBS were injected into the tail vein of 8- to 11-week-old host mice. After 2 weeks, the animals were killed, and the lungs were removed and fixed in Bouin's solution or 4% paraformaldehyde. Lung occupancy by visible B16F10 tumor colonies was analyzed using NIH ImageJ. E0771 cells (5.0×10^5) were injected subcutaneously into the mammary fat pad. Tumor volume (in mm^3) was measured with calipers and calculated as $(w^2 \times l)/2$. For stable expression of tdTomato, E0771 cells were infected with a lentivirus encoding MYC epitope–tagged tdTomato for 2 days. Mice were fed normal chow without or with supplementation with 0.005% propagermanium (3-oxygemylpropinic acid polymer; provided by Sanwa Kagaku Kenkyusho Co.) beginning 1 day before cancer cell injection. Experiments were randomized, and investigators were blinded during experiments in the animal studies.

Cell culture. B16F10 (provided by Cell Resource Center of Tohoku University), LLC (provided by Cell Resource Center of Tohoku University), B16F1 (provided by S. Okano, Kyushu University, Fukuoka, Japan), and E0771 (CH3 BioSystems) cells were maintained in RPMI 1640 medium (Sigma-Aldrich) supplemented with 10% fetal bovine serum (Invitrogen), 1 mM sodium pyruvate, 100 U/ml penicillin, 100 μg/ml streptomycin, 2 mM L-glutamine, and 10 ml/l nonessential amino acids (Gibco). BMSCs were isolated from BM collected from the tibia and femur of 8- to 10-week-old mice, and they were cultured in RPMI 1640 medium supplemented with 10% fetal bovine serum, 10% horse serum, 2 mM L-glutamine, 100 U/ml penicillin, and 100 μg/ml streptomycin. Nonadherent cells were removed after 24 hours, and adherent cells were maintained with replenishment of the medium every 3 days. BMSCs were treated with 10 μM tamoxifen (Sigma-Aldrich) for 2 days in order to delete floxed *Fbxw7* alleles. They were also treated with DAPT (Calbiochem) for 2 days to inhibit NOTCH signaling. MEFs were prepared from embryos at embryonic day 13.5 and maintained as previously described (65), and they were treated with 2 μM tamoxifen (Sigma-Aldrich) for 2 days in order to delete floxed *Fbxw7* alleles.

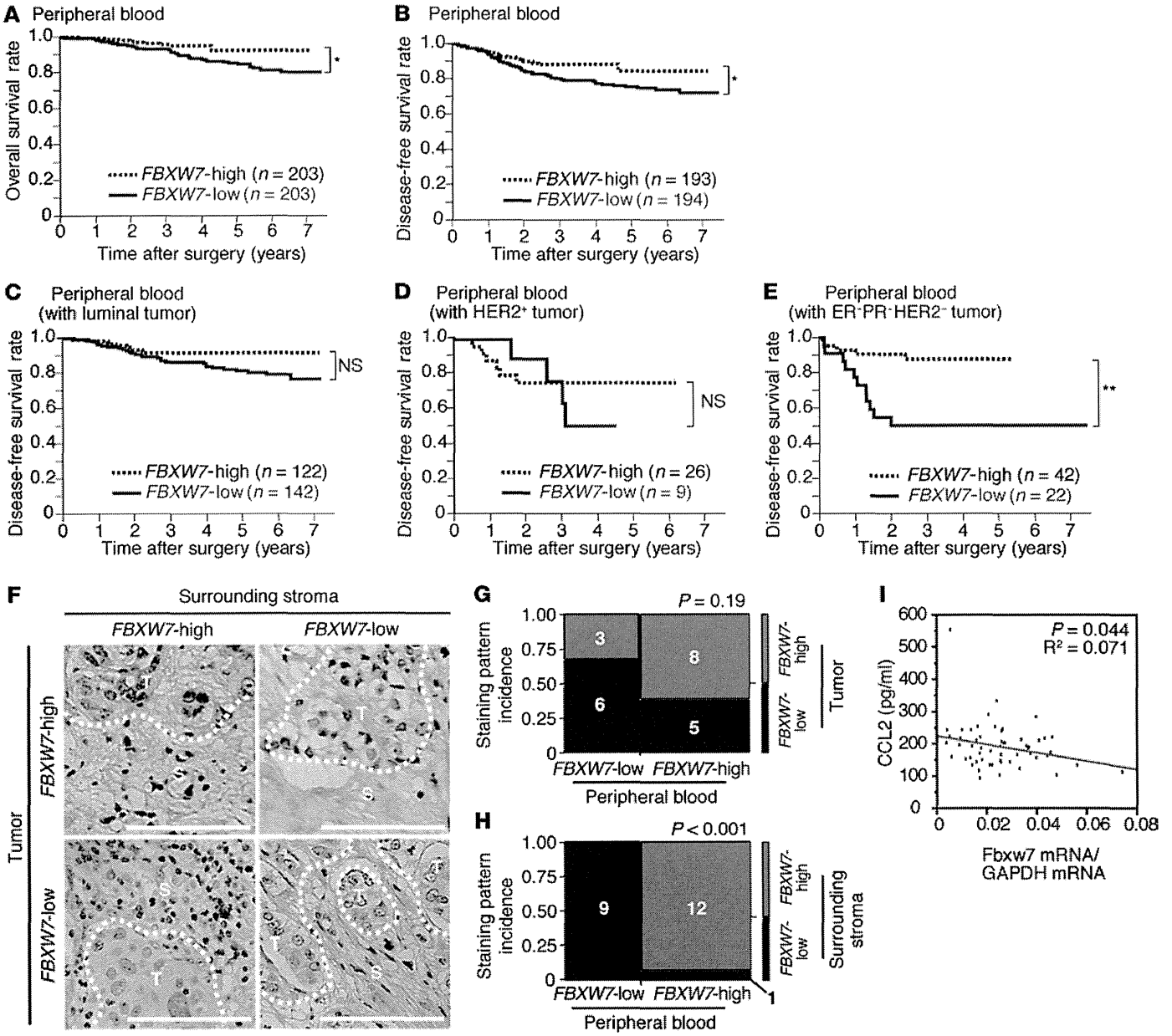

Figure 7. Clinical relevance of FBXW7 expression in breast cancer patients. (**A** and **B**) Kaplan-Meier curves for overall (**A**) and disease-free (**B**) survival of breast cancer patients (n = 406) classified according to the abundance of *FBXW7* mRNA in peripheral blood. (**C**–**E**) Kaplan-Meier curves for disease-free survival of breast cancer patients with luminal (**C**), HER2$^+$ (**D**), or triple-negative ER$^-$PR$^-$HER2$^-$ (**E**) tumors classified according to the abundance of *FBXW7* mRNA in peripheral blood. $^*P < 0.05$, $^{**}P < 0.01$, log-rank test. (**F**) Representative immunohistochemical staining patterns for FBXW7 in breast cancer patients: positive in both primary tumor cells and stroma, positive in tumor cells only, positive in stroma only, or negative in both tumor cells and stroma. T, tumor cells; S, surrounding stromal cells. Scale bars: 100 μm. (**G** and **H**) Mosaic plots summarizing the abundance of *FBXW7* mRNA in peripheral blood and *FBXW7* expression in tumor cells (**G**) and surrounding stroma (**H**) for the indicated numbers of breast cancer patients (n = 22). P values for the association between these parameters were calculated by χ^2 test. (**I**) Correlation between the abundance of *FBXW7* mRNA in peripheral blood and the serum CCL2 concentration in breast cancer patients (n = 57).

Flow cytometry. For sorting of peripheral blood cells of breast cancer patients, we obtained 6 ml heparinized peripheral blood from 4 patients with recurrent breast cancer and metastasis. Mononuclear cells were isolated from the blood by Ficoll (GE Healthcare) density centrifugation at 500 *g* for 25 minutes at 4°C. Erythrocytes were lysed with 1× BD Pharm Lyse buffer (BD Biosciences). The isolated cells were then stained with antibodies against CD45 (clone HI100, Sony Biotechnology) and CD326 (clone 9C4, Sony Biotechnology) for analysis using Cell Sorter SH800 (Sony Biotechnology). For analysis of mouse BM and peripheral blood, erythrocytes were lysed with hemolysis buffer (0.14 M NH_4Cl and 0.01 M Tris-HCl at pH 7.5), and the remaining cells were stained with antibodies against F4/80 (clone BM8, eBioscience), CD115 (clone AFS98, eBioscience), MAC1 (clone M1/70, eBioscience), Ly6G (clone 1A8, BD Biosciences), and Ly6C (clone AL-21, BD Biosciences). The stained cells were analyzed with a FACSCalibur flow cytometer (BD).

Histological, immunohistochemical, and immunohistofluorescence analyses. For H&E staining, tissue was fixed in Bouin's solution, embedded in paraffin, cut into serial sections (4 μm thickness),

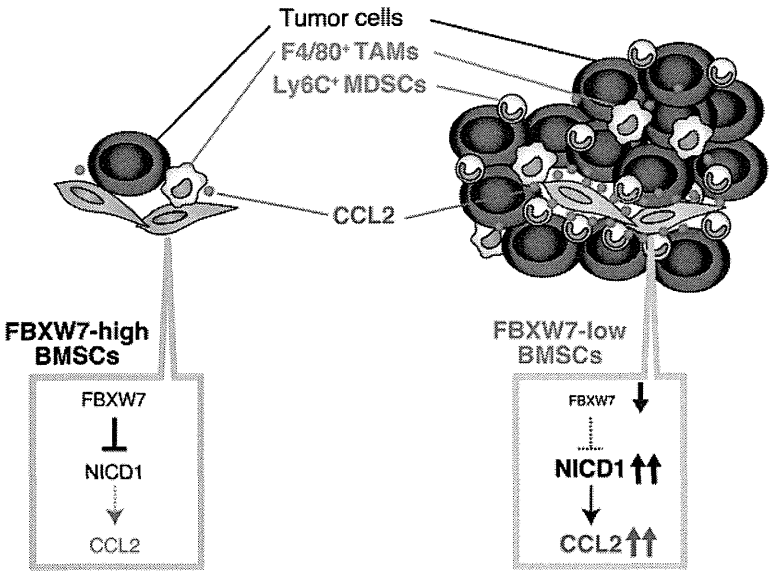

Figure 8. Promotion of cancer metastasis by loss of FBXW7 in the host environment. Loss of FBXW7 in BMSCs results in accumulation of NICD1 and increased secretion of CCL2, which in turn promotes recruitment of Mo-MDSCs and macrophages. These cells then promote the growth of tumors that have already colonized the lungs. TAM, tumor-associated macrophage.

and stained as described previously (66). For immunohistochemical analysis, breast tissue microarray slides obtained from Kyushu University Beppu Hospital were stained with antibodies against FBXW7 (clone 3D1, Abnova) using an Envision immunostaining system (DAKO). The sections were counterstained with hematoxylin. Immunohistochemical staining intensity of breast cancer regions and surrounding stroma was scored as negative (low) or positive (high). For immunohistofluorescence analysis, tissue was fixed with 4% paraformaldehyde in 0.1 M phosphate buffer, embedded in 30% sucrose overnight, sectioned (15 μm thickness) with a cryostat, and stained as described previously (66). Antibodies against TCRβ (clone H57-597), B220 (clone RA3-6B2), MAC1 (clone M1/70), and c-Kit (clone 2B8) were from eBioscience; antibodies against Ly6C (clone AL-21), Ly6G (clone 1A8), and VE-cadherin (clone 11D4.1) were from BD Biosciences; antibodies against F4/80 (clone A3-1) were from Serotec; and antibodies against FSP (clone D9F9D) were from Cell Signaling Technology. Immune complexes were detected with secondary antibodies labeled with Alexa Fluor 633 or Alexa Fluor 405 (Molecular Probes), each at a dilution of 1:2,000. The sections were mounted in Fluoromount (Diagnostic BioSystems) and examined with a laser-scanning confocal microscope (LSM700, Carl Zeiss).

Immunoblot analysis. Total protein extracts were prepared from BMSCs with lysis buffer (50 mM Tris-HCl, pH 7.5; 150 mM NaCl; 0.5% Triton X-100; 10 mM NaF; 10 mM $Na_4P_2O_7$; 0.4 mM Na_3VO_4; 0.4 mM EDTA; 20 μg/ml leupeptin; 10 μg/ml aprotinin; 1 mM phenylmethylsulfonyl fluoride). The extracts (20 μg protein) were subjected to immunoblot analysis as previously described (67). Antibodies against NOTCH3 (clone M-20) and KLF5 (clone H-300) were obtained from Santa Cruz Biotechnology; antibodies against cleaved NOTCH1 (clone D1E11), NOTCH2 (clone D76A6), c-JUN (clone 60A8), p100-p52 (catalog no. 4882), and mTOR (clone 7C10) were from Cell Signaling Technology; antibodies against c-MYC were from Abcam; and antibodies against GAPDH (loading control) were from BD Biosciences.

Retroviral expression system. Complementary DNA encoding hemagglutinin epitope–tagged mouse NICD1, mouse c-MYC, mouse KLF5, or FLAG epitope–tagged mouse FBXW7α (or its ΔF mutant) were subcloned into pMX-puro (provided by T. Kitamura, University of Tokyo, Tokyo, Japan), and the resulting vectors were used to transfect Plat E cells (68) and thereby generate recombinant retroviruses. BMSCs were infected with recombinant retroviruses and subjected to selection in medium containing puromycin (10 μg/ml). Cells stably expressing each recombinant protein were pooled for experiments.

RNAi. Construction of shRNA vectors and RNAi were performed as described previously (69). The sequence targeted for mouse *Ccl2* was 5′-GGTATTCCCTTTCATGAATAC-3′. An RNAi vector for EGFP was used as a control.

RT and real-time PCR analysis. Total RNA (1 μg), isolated from mouse cells using Isogen (Nippon Gene), was subjected to RT with a QuantiTect Reverse Transcription Kit (Qiagen), and the resulting cDNA was subjected to real-time PCR analysis with SYBR Green PCR Master Mix and specific primers in a StepOnePlus Real-Time PCR System (Applied Biosystems). PCR primer sequences were as follows: *Ccl2* sense, 5′-CAGCAGCAGGTGTCCCAAAG-3′; *Ccl2* antisense, 5′-TGTCTGGACCCATTCCTTCTTG-3′; *Rps18* sense, 5′-GAGGACCTGGAGAGGCTGAAG-3′; *Rps18* antisense, 5′-CTGCGGCCAGTGGTCTTG-3′. The amount of *Ccl2* mRNA was normalized to that of *Rps18* mRNA. For human clinical specimens, total RNA (2.7 μg) isolated from cells using Isogen-LS (Nippon Gene) was subjected to RT with Moloney leukemia virus reverse transcriptase (BRL), and the resulting cDNA was subjected to real-time PCR analysis with SYBR-Green I dye and specific primers in a LightCycler system (Roche Applied Science). Amplification was monitored as described previously (70). PCR primer sequences were as follows: *Fbxw7* sense, 5′-CCTCCAGGAATGGCTAAAAA-3′; *Fbxw7* antisense, 5′-AAGAGTTCATCTAAAGCAAGCAA-3′; *Gapdh* sense, 5′-AGCCACATCGCTCAGACAC-3′; *Gapdh* antisense, 5′-GCCCAATACGACCAAATCC-3′. The amount of *Fbxw7* mRNA was normalized to that of *Gapdh* mRNA.

Antibody array and ELISA. The serum concentrations of chemokines and cytokines were analyzed using a Proteome Profiler kit (catalog nos. ARY006 and ARY015, R&D Systems). CCL2 levels in mouse or human serum and in mouse BMSC or MEF culture supernatants were also measured by ELISA (Ready-SET-Go kit; eBioscience). For measurement of CCL2 release by BMSCs or MEFs, cells (1×10^4 per well in 24-well plates) were cultured for 48 hours.

Luciferase reporter assay. The promoter region of mouse *Ccl2* and its deletion mutants were subcloned into pGL2-Basic (Promega), which encodes firefly luciferase. BMSCs were seeded (2×10^4 per well in 24-well plates) 24 hours before transfection with promoter constructs (0.25 μg) and the internal control vector pRL-TK (0.25 μg; Promega) for *Renilla* luciferase using the FuGENE HD reagent (Promega). Luciferase activities were measured using a Dual-Luciferase Reporter Assay System (Promega) and a Lumat LB9507 luminometer (EG&G Berthold) at 48 hours after transfection. Firefly luciferase activity was normalized to that of *Renilla* luciferase.

ChIP. BMSCs (2×10^7) were fixed for 5 minutes with 0.5% formaldehyde in RPMI1640 medium. Fixation was terminated by addition of glycine to a final concentration of 0.125 M, and cells were then washed with ice-cold PBS, lysed with 2 ml lysis buffer (5 mM Hepes-NaOH, pH 8.0; 200 mM KCl; 1 mM $CaCl_2$; 1.5 mM $MgCl_2$; 5% sucrose; and 0.5% Nonidet P-40) and exposed to micrococcal nuclease (New England Biolabs) to yield chromatin fragments consisting of 1–5 nucleosomes. The nucleosomes were incubated for 6 hours at 4°C with 2 μg of antibodies against NOTCH1 (clone C-20, Santa Cruz Biotechnology) conjugated to 20 μl Dynabeads–Protein G. The immunoprecipitated material was washed, chromatin was eluted, and the crosslinks were reversed. The DNA fragments were purified by phenol-chloroform extraction followed by precipitation with isopropanol, then used as a template for real-time PCR analysis with the SYBR Select PCR system (Applied Biosystems). PCR primer sequences were as follows: *Ccl2* (distal) sense, 5′-GCTCACATTCCAGCTAAATATCTCT-3′; *Ccl2* (distal) antisense, 5′-GAGTTATTGTCTGTTTCCCTCTCA-3′; *Ccl2* (proximal) sense, 5′-TTACTGGGGGTCCTTTCCCA-3′; *Ccl2* (proximal) antisense, 5′-GGAGTGGCTCTGCTTTCACT-3′. The extent of chromatin enrichment was normalized to input.

Statistics. Quantitative data were subjected to statistical analysis as indicated. A *P* value less than 0.05 was considered statistically significant.

Study approval. All animal experiments were approved by the IACUC of Kyushu University, and animal care was in accordance with institutional guidelines. All clinical samples were approved for analysis by the ethical committees of the National Hospital Organization Kyushu Cancer Center (no. 2001-15; October 16, 2001) and Kyushu University (no. 302; February 9, 2006). Written informed consent was obtained from all patients with cancers analyzed in this study.

Acknowledgments

We thank T. Honjo for *RbpJκ*$^{fl/fl}$ mice; I.M. de Alborán for *c-Myc*$^{fl/fl}$ mice; K. Rajewsky for *Mx1-Cre* transgenic mice; M. Okabe for *CAG-EGFP* transgenic mice; S. Okano for B16F1 melanoma cells; T. Kitamura for pMX-puro; Sanwa Kagaku Kenkyusho Co. for propagermanium; A. Kataoka for collection of BM and peripheral blood from breast cancer patients; S. Tokunaga for comments on statistical analysis; Y. Tateishi, S. Yamamura, K. Watanabe, N. Nishimura, K. Tsunematsu, A. Niihara, M. Tanaka, K. Motomura, and N. Kinoshita for technical assistance; members of our laboratories for comments on the manuscript; and A. Ohta for help with manuscript preparation. This work was supported in part by a grant from the Project for Development of Innovative Research on Cancer Therapeutics (P-DIRECT).

Address correspondence to: Keiichi I. Nakayama, Department of Molecular and Cellular Biology, Medical Institute of Bioregulation, Kyushu University, 3-1-1 Maidashi, Higashi-ku, Fukuoka, Fukuoka 812-8582, Japan. Phone: 81.92.642.6815; E-mail: nakayak1@bioreg.kyushu-u.ac.jp.

1. Fridman WH, Pages F, Sautes-Fridman C, Galon J. The immune contexture in human tumours: impact on clinical outcome. *Nat Rev Cancer*. 2012;12(4):298–306.
2. de Visser KE, Korets LV, Coussens LM. De novo carcinogenesis promoted by chronic inflammation is B lymphocyte dependent. *Cancer Cell*. 2005;7(5):411–423.
3. Murdoch C, Muthana M, Coffelt SB, Lewis CE. The role of myeloid cells in the promotion of tumour angiogenesis. *Nat Rev Cancer*. 2008;8(8):618–631.
4. Youn JI, Nagaraj S, Collazo M, Gabrilovich DI. Subsets of myeloid-derived suppressor cells in tumor-bearing mice. *J Immunol*. 2008;181(8):5791–5802.
5. Khaled YS, Ammori BJ, Elkord E. Myeloid-derived suppressor cells in cancer: recent progress and prospects. *Immunol Cell Biol*. 2013;91(8):493–502.
6. Talmadge JE, Gabrilovich DI. History of myeloid-derived suppressor cells. *Nat Rev Cancer*. 2013;13(10):739–752.
7. Bingle L, Brown NJ, Lewis CE. The role of tumour-associated macrophages in tumour progression: implications for new anticancer therapies. *J Pathol*. 2002;196(3):254–265.
8. Mosser DM, Edwards JP. Exploring the full spectrum of macrophage activation. *Nat Rev Immunol*. 2008;8(12):958–969.
9. Qian BZ, Pollard JW. Macrophage diversity enhances tumor progression and metastasis. *Cell*. 2010;141(1):39–51.
10. Siveen KS, Kuttan G. Role of macrophages in tumour progression. *Immunol Lett*. 2009;123(2):97–102.
11. Karnoub AE, et al. Mesenchymal stem cells within tumour stroma promote breast cancer metastasis. *Nature*. 2007;449(7162):557–563.
12. Hanahan D, Coussens LM. Accessories to the crime: functions of cells recruited to the tumor microenvironment. *Cancer Cell*. 2012;21(3):309–322.
13. Kaplan RN, et al. VEGFR1-positive haematopoietic bone marrow progenitors initiate the pre-metastatic niche. *Nature*. 2005;438(7069):820–827.
14. Gao D, et al. Endothelial progenitor cells control the angiogenic switch in mouse lung metastasis. *Science*. 2008;319(5860):195–198.
15. Joyce JA, Pollard JW. Microenvironmental regulation of metastasis. *Nat Rev Cancer*. 2009;9(4):239–252.
16. Balkwill F. Cancer and the chemokine network. *Nat Rev Cancer*. 2004;4(7):540–550.
17. Mukaida N, Baba T. Chemokines in tumor development and progression. *Exp Cell Res*. 2011;318(2):95–102.
18. Van Coillie E, Van Damme J, Opdenakker G. The MCP/eotaxin subfamily of CC chemokines. *Cytokine Growth Factor Rev*. 1999;10(1):61–86.
19. Qian BZ, et al. CCL2 recruits inflammatory monocytes to facilitate breast-tumour metastasis. *Nature*. 2011;475(7355):222–225.
20. Salcedo R, et al. Human endothelial cells express CCR2 and respond to MCP-1: direct role of MCP-1 in angiogenesis and tumor progression. *Blood*. 2000;96(1):34–40.
21. Loberg RD, et al. Targeting CCL2 with systemic delivery of neutralizing antibodies induces prostate cancer tumor regression in vivo. *Cancer Res*. 2007;67(19):9417–9424.
22. Zhu X, Fujita M, Snyder LA, Okada H. Systemic delivery of neutralizing antibody targeting CCL2 for glioma therapy. *J Neurooncol*. 2011;104(1):83–92.
23. Lu X, Kang Y. Chemokine (C-C motif) ligand 2 engages CCR2+ stromal cells of monocytic origin to promote breast cancer metastasis to lung and bone. *J Biol Chem*. 2009;284(42):29087–29096.
24. Welcker M, et al. The Fbw7 tumor suppressor regulates glycogen synthase kinase 3 phosphorylation-dependent c-Myc protein degradation. *Proc Natl Acad Sci U S A*. 2004;101(24):9085–9090.
25. Yada M, et al. Phosphorylation-dependent degradation of c-Myc is mediated by the F-box protein Fbw7. *EMBO J*. 2004;23(10):2116–2125.
26. Hubbard EJ, Wu G, Kitajewski J, Greenwald I. sel-10, a negative regulator of lin-12 activity in Caenorhabditis elegans, encodes a member of the CDC4 family of proteins. *Genes Dev*. 1997;11(23):3182–3193.
27. Gupta-Rossi N, et al. Functional interaction between SEL-10, an F-box protein, and the nuclear form of activated Notch1 receptor. *J Biol Chem*. 2001;276(37):34371–34378.
28. Oberg C, et al. The Notch intracellular domain is ubiquitinated and negatively regulated by the mammalian Sel-10 homolog. *J Biol Chem*. 2001;276(38):35847–35853.
29. Koepp DM, et al. Phosphorylation-dependent ubiquitination of cyclin E by the SCFFbw7 ubiquitin ligase. *Science*. 2001;294(5540):173–177.
30. Moberg KH, Bell DW, Wahrer DC, Haber DA, Hariharan IK. Archipelago regulates Cyclin E levels in Drosophila and is mutated in human cancer cell lines. *Nature*. 2001;413(6853):311–316.
31. Strohmaier H, et al. Human F-box protein hCdc4 targets cyclin E for proteolysis and is mutated in a breast cancer cell line. *Nature*. 2001;413(6853):316–322.

32. Nateri AS, Riera-Sans L, Da Costa C, Behrens A. The ubiquitin ligase SCFFbw7 antagonizes apoptotic JNK signaling. *Science*. 2004;303(5662):1374–1378.
33. Wei W, Jin J, Schlisio S, Harper JW, Kaelin WG Jr. The v-Jun point mutation allows c-Jun to escape GSK3-dependent recognition and destruction by the Fbw7 ubiquitin ligase. *Cancer Cell*. 2005;8(1):25–33.
34. Liu N, et al. The Fbw7/human CDC4 tumor suppressor targets proproliferative factor KLF5 for ubiquitination and degradation through multiple phosphodegron motifs. *J Biol Chem*. 2010;285(24):18858–18867.
35. Zhao D, Zheng HQ, Zhou Z, Chen C. The Fbw7 tumor suppressor targets KLF5 for ubiquitin-mediated degradation and suppresses breast cell proliferation. *Cancer Res*. 2010;70(11):4728–4738.
36. Mao JH, et al. FBXW7 targets mTOR for degradation and cooperates with PTEN in tumor suppression. *Science*. 2008;321(5895):1499–1502.
37. Akhoondi S, et al. FBXW7/hCDC4 is a general tumor suppressor in human cancer. *Cancer Res*. 2007;67(19):9006–9012.
38. Onoyama I, et al. Conditional inactivation of Fbxw7 impairs cell-cycle exit during T cell differentiation and results in lymphomatogenesis. *J Exp Med*. 2007;204(12):2875–2888.
39. Matsuoka S, et al. Fbxw7 acts as a critical fail-safe against premature loss of hematopoietic stem cells and development of T-ALL. *Genes Dev*. 2008;22(8):986–991.
40. Thompson BJ, et al. The SCFFBW7 ubiquitin ligase complex as a tumor suppressor in T cell leukemia. *J Exp Med*. 2007;204(8):1825–1835.
41. Babaei-Jadidi R, et al. FBXW7 influences murine intestinal homeostasis and cancer, targeting Notch, Jun, and DEK for degradation. *J Exp Med*. 2011;208(2):295–312.
42. Nakayama KI, Nakayama K. Ubiquitin ligases: cell-cycle control and cancer. *Nat Rev Cancer*. 2006;6(5):369–381.
43. Welcker M, Clurman BE. FBW7 ubiquitin ligase: a tumour suppressor at the crossroads of cell division, growth and differentiation. *Nat Rev Cancer*. 2008;8(2):83–93.
44. Wang Z, et al. Tumor suppressor functions of FBW7 in cancer development and progression. *FEBS Lett*. 2012;586(10):1409–1418.
45. Molloy AP, et al. Mesenchymal stem cell secretion of chemokines during differentiation into osteoblasts, and their potential role in mediating interactions with breast cancer cells. *Int J Cancer*. 2009;124(2):326–332.
46. Shi C, et al. Bone marrow mesenchymal stem and progenitor cells induce monocyte emigration in response to circulating toll-like receptor ligands. *Immunity*. 2011;34(4):590–601.
47. Allers C, et al. Dynamic of distribution of human bone marrow-derived mesenchymal stem cells after transplantation into adult unconditioned mice. *Transplantation*. 2004;78(4):503–508.
48. Ling PD, Rawlins DR, Hayward SD. The Epstein-Barr virus immortalizing protein EBNA-2 is targeted to DNA by a cellular enhancer-binding protein. *Proc Natl Acad Sci U S A*. 1993;90(20):9237–9241.
49. Ross DA, Kadesch T. The notch intracellular domain can function as a coactivator for LEF-1. *Mol Cell Biol*. 2001;21(22):7537–7544.
50. Inuzuka H, et al. SCFFBW7 regulates cellular apoptosis by targeting MCL1 for ubiquitylation and destruction. *Nature*. 2011;471(7336):104–109.
51. Wertz IE, et al. Sensitivity to antitubulin chemotherapeutics is regulated by MCL1 and FBW7. *Nature*. 2011;471(7336):110–114.
52. Balamurugan K, et al. The tumour suppressor C/EBPδ inhibits FBXW7 expression and promotes mammary tumour metastasis. *EMBO J*. 2010;29(24):4106–4117.
53. Cushing SD, et al. Minimally modified low density lipoprotein induces monocyte chemotactic protein 1 in human endothelial cells and smooth muscle cells. *Proc Natl Acad Sci U S A*. 1990;87(13):5134–5138.
54. Standiford TJ, Kunkel SL, Phan SH, Rollins BJ, Strieter RM. Alveolar macrophage-derived cytokines induce monocyte chemoattractant protein-1 expression from human pulmonary type II-like epithelial cells. *J Biol Chem*. 1991;266(15):9912–9918.
55. Lu Y, et al. PTHrP-induced MCP-1 production by human bone marrow endothelial cells and osteoblasts promotes osteoclast differentiation and prostate cancer cell proliferation and invasion in vitro. *Int J Cancer*. 2007;121(4):724–733.
56. Silzle T, et al. Tumor-associated fibroblasts recruit blood monocytes into tumor tissue. *Eur J Immunol*. 2003;33(5):1311–1320.
57. Kuhn R, Schwenk F, Aguet M, Rajewsky K. Inducible gene targeting in mice. *Science*. 1995;269(5229):1427–1429.
58. Tanigaki K, et al. Regulation of αβ/γδ T cell lineage commitment and peripheral T cell responses by Notch/RBP-J signaling. *Immunity*. 2004;20(5):611–622.
59. de Alboran IM, et al. Analysis of C-MYC function in normal cells via conditional gene-targeted mutation. *Immunity*. 2001;14(1):45–55.
60. Wolfer A, Wilson A, Nemir M, MacDonald HR, Radtke F. Inactivation of Notch1 impairs VDJβ rearrangement and allows pre-TCR-independent survival of early αβ lineage thymocytes. *Immunity*. 2002;16(6):869–879.
61. Clausen BE, Burkhardt C, Reith W, Renkawitz R, Forster I. Conditional gene targeting in macrophages and granulocytes using LysMcre mice. *Transgenic Res*. 1999;8(4):265–277.
62. Rickert RC, Roes J, Rajewsky K. B lymphocyte-specific, Cre-mediated mutagenesis in mice. *Nucleic Acids Res*. 1997;25(6):1317–1318.
63. Hayashi S, McMahon AP. Efficient recombination in diverse tissues by a tamoxifen-inducible form of Cre: a tool for temporally regulated gene activation/inactivation in the mouse. *Dev Biol*. 2002;244(2):305–318.
64. Okabe M, Ikawa M, Kominami K, Nakanishi T, Nishimune Y. 'Green mice' as a source of ubiquitous green cells. *FEBS Lett*. 1997;407(3):313–319.
65. Nakayama K, et al. Mice lacking p27Kip1 display increased body size, multiple organ hyperplasia, retinal dysplasia, and pituitary tumors. *Cell*. 1996;85(5):707–720.
66. Nakayama K, et al. Targeted disruption of Skp2 results in accumulation of cyclin E and p27Kip1, polyploidy and centrosome overduplication. *EMBO J*. 2000;19(9):2069–2081.
67. Kamura T, et al. Degradation of p57Kip2 mediated by SCFSkp2-dependent ubiquitylation. *Proc Natl Acad Sci U S A*. 2003;100(18):10231–10236.
68. Morita S, Kojima T, Kitamura T. Plat-E: an efficient and stable system for transient packaging of retroviruses. *Gene Ther*. 2000;7(12):1063–1066.
69. Kamura T, et al. Cytoplasmic ubiquitin ligase KPC regulates proteolysis of p27Kip1 at G1 phase. *Nat Cell Biol*. 2004;6(12):1229–1235.
70. Nagahara H, et al. Clinicopathologic and biological significance of kallikrein 6 overexpression in human gastric cancer. *Clin Cancer Res*. 2005;11(19 pt 1):6800–6806.

Nucleic Acids Research Advance Access published August 8, 2014

Nucleic Acids Research, 2014 **1**
doi: 10.1093/nar/gku652

ZFP36L1 and ZFP36L2 control LDLR mRNA stability via the ERK–RSK pathway

Shungo Adachi[1,2], Masae Homoto[1], Rikou Tanaka[1,2], Yusaku Hioki[1], Hiroshi Murakami[3], Hiroaki Suga[4], Masaki Matsumoto[5], Keiichi I. Nakayama[5], Tomohisa Hatta[1], Shun-ichiro Iemura[1] and Tohru Natsume[1,*]

[1]Molecular Profiling Research Center for Drug Discovery (molprof), National Institute of Advanced Industrial Science and Technology (AIST), Tokyo 135-0064, Japan, [2]Galaxy Pharma Inc., Akita 010-0951, Japan, [3]Department of Life Sciences, Graduate School of Arts and Sciences, The University of Tokyo, Meguro-ku, Tokyo 153-8904, Japan, [4]Department of Chemistry, Graduate School of Science, The University of Tokyo, 7-3-1 Bunkyo-ku, Tokyo 113-0033, Japan and [5]Department of Molecular and Cellular Biology, Medical Institute of Bioregulation, Kyushu University, Fukuoka 812-8582, Japan

Received August 20, 2013; Revised July 06, 2014; Accepted July 7, 2014

ABSTRACT

Low-density lipoprotein receptor (LDLR) mRNA is unstable, but is stabilized upon extracellular signal-regulated kinase (ERK) activation, possibly through the binding of certain proteins to the LDLR mRNA 3′-untranslated region (UTR), although the detailed mechanism underlying this stability control is unclear. Here, using a proteomic approach, we show that proteins ZFP36L1 and ZFP36L2 specifically bind to the 3′-UTR of LDLR mRNA and recruit the CCR4-NOT-deadenylase complex, resulting in mRNA destabilization. We also show that the C-terminal regions of ZFP36L1 and ZFP36L2 are directly phosphorylated by p90 ribosomal S6 kinase, a kinase downstream of ERK, resulting in dissociation of the CCR4-NOT-deadenylase complex and stabilization of LDLR mRNA. We further demonstrate that targeted disruption of the interaction between LDLR mRNA and ZFP36L1 and ZFP36L2 using antisense oligonucleotides results in upregulation of LDLR mRNA and protein. These results indicate that ZFP36L1 and ZFP36L2 regulate LDLR protein levels downstream of ERK. Our results also show the usefulness of our method for identifying critical regulators of specific RNAs and the potency of antisense oligonucleotide-based therapeutics.

INTRODUCTION

Messenger RNA (mRNA) turnover plays a key role in the regulation of protein levels. This regulation is achieved through *cis*-regulatory elements, including adenosine and uridine (AU)-rich elements (AREs) residing in the 3′-untranslated regions (UTRs) of mRNAs. AREs are present in many translationally repressed and unstable mRNA species and play a role in 5–8% of all mRNAs (1). Destabilization of ARE-containing mRNAs is accomplished through their interaction with ARE-binding proteins (ARE-BPs). Many ARE-BPs, including hnRNPD, KHSRP, DHX36 and ZFP36 family proteins have been identified (2); however, predicting which protein can bind to a specific ARE is still very difficult (2).

The low-density lipoprotein (LDL) receptor (LDLR) is a receptor for circulating LDL and has a critical role in removing LDL from blood (3). A high blood level of LDL cholesterol is a major risk factor for heart disease. Development of a drug to increase the amount of LDLR protein in the liver to lower LDL cholesterol is advanced and would be highly beneficial (3).

LDLR mRNA is known to be unstable, but is stabilized upon phorbol 12-myristate 13-acetate (PMA) treatment through the activation of extracellular signal-regulated kinase (ERK) (4). The 3′-UTR of LDLR mRNA, particularly the 1 kb 5′ region that contains three AREs (ARE1–3), and the proteins that bind this region are thought to be involved in this stabilization. Although some LDLR mRNA-binding proteins have been identified, the detailed mechanisms underlying the control of LDLR mRNA stability remain unknown (4,5), and the critical regulator of this control has not been identified.

Here, using a proteomic approach, we found that ZFP36L1 and ZFP36L2 bind specifically to the LDLR mRNA 3′-UTR region. ZFP36L1 and ZFP36L2 belong to the family of CCCH tandem zinc finger proteins (the ZFP36 family, which includes ZFP36, ZFP36L1 and ZFP36L2)

*To whom correspondence should be addressed. Tel: +81 3 3599 8140; Fax: +81 3 3599 8134; Email: t-natsume@aist.go.jp
Present address: Shun-ichiro Iemura, Translational Research Center, Fukushima Medical University, 11-25 Sakaemachi, Fukushima 960-8031, Japan.

(6). ZFP36 family proteins bind to AREs and trigger the degradation of several ARE-containing mRNAs, including PLK3 and vascular endothelial growth factor A (VEGFA) (7,8). We examined the role of ZFP36L1 and ZFP36L2 in LDLR mRNA stability using an RNAi-based knockdown method and we found that ZFP36L1 and ZFP36L2 destabilize LDLR mRNA. We also found that p90 ribosomal S6 kinase (RSK)1, a kinase downstream of ERK, directly phosphorylates the C-terminus of ZFP36L1 and inhibits the mRNA-destabilizing activity of ZFP36L1. From these results, we conclude that ZFP36L1 and ZFP36L2 regulate the levels of LDLR protein downstream of ERK.

We then tried to disrupt the interaction between LDLR-mRNA and ZFP36L1 and ZFP36L2 proteins using locked nucleic acid (LNA)- (9) modified antisense oligonucleotides. We were able to selectively disrupt the interaction between LDLR-mRNA and ZFP36L1 and ZFP36L2 without affecting interactions of ZFP36L1 and ZFP36L2 with other target mRNAs. This resulted in an increase in LDLR protein levels. Our results show the usefulness of our method for identifying regulators of specific mRNAs and also show the potency of antisense oligonucleotide-based therapeutics.

MATERIALS AND METHODS

Cell culture

HEK293T and HeLa cells were cultured at 37°C in Dulbecco's modified Eagle's medium supplemented with 10% fetal bovine serum. Hep3B cells were cultured at 37°C in minimal essential medium supplemented with nonessential amino acids and 10% fetal bovine serum.

Preparation of bait RNAs

T7 tagged cDNA template was polymerase chain reaction (PCR) amplified and subjected to *in vitro* transcription using a MEGAscript T7 kit (Applied Biosystems). Amplified cRNA was purified with an RNeasy Mini Kit (Qiagen) and then subjected to Flag conjugation as described (10) with some modifications. Briefly, 60 μl of freshly prepared 0.1 M $NaIO_4$ was added to 60 μl of 250 pmol cRNA, and the mixture was incubated at 0°C for 10 min. The 3′dialdehyde RNA was precipitated with 1 ml of 2% $LiClO_4$ in acetone followed by washing with 1 ml acetone. The pellet was dissolved in 10 μl of 0.1 M sodium acetate, pH 5.2 and then mixed with 12 μl of 30 mM hydrazide–Flag peptide. The reaction solution was mixed at room temperature for 30 min. The resulting imine-moiety of the cRNA was reduced by adding 12 μl of 1 M $NaCNBH_3$, and then incubated at room temperature for 30 min. The RNA was purified with an RNeasy Mini Kit (Qiagen). The regions of bait RNAs used for immunoprecipitation (IP) experiments are shown in Supplemental Table IV.

Purification and analysis of RNA-binding protein

Purification and analysis of RNA-binding protein (RBP) were carried out as described (11) with some modifications. Briefly, 293T cells were lysed with lysis buffer [10 mM 4-(2-hydroxyethyl)-1-piperazineethanesulfonic acid (HEPES) (pH 7.5), 150 mM NaCl, 50 mM NaF, 1 mM Na_3VO_4, 5 μg/ml leupeptin, 5 μg ml aprotinin, 3 μg/ml pepstatin A, 1 mM phenylmethylsulfonyl fluoride (PMSF), 1 mg/ml digitonin] and cleared by centrifugation. The cleared lysate was incubated with indicated amounts of Flag-tagged bait RNA, antisense oligos and Flag-M2-conjugated agarose for 1 h. The agarose resin was then washed three times with wash buffer [10 mM HEPES (pH 7.5), 150 mM NaCl, 0.1% Triton X-100] and co-immunoprecipitated RNA and proteins were eluted with Flag elution buffer [0.5 mg/ml Flag peptide, 10 mM HEPES (pH 7.5), 150 mM NaCl, 0.05% Triton X-100]. The bait RNA associated proteins were digested with lysyl endopeptidase, and the resulting peptides were analyzed using a nanoscale liquid-chromatography tandem mass spectrometry (LC/MS/MS) system.

Western blot analysis

Whole-cell lysates or immunoprecipitates were resolved by sodium dodecyl sulphate (SDS) polyacrylamide gel electrophoresis and then transferred onto Immobilon-P membranes (Millipore). The membranes were probed with the indicated antibodies and proteins of interest were visualized with horseradish peroxidase-conjugated mouse, rabbit or goat immunoglobulin G using ECL Plus (GE). Intensity of individual bands was quantified using Multi Gauge software (Fuji Photo Film).

Quantitative reverse-transcription PCR

Total RNA was purified using the RNeasy Mini Kit (Qiagen). cDNA was synthesized using the High Capacity cDNA Reverse Transcription Kit (Invitrogen). Quantitative PCR (qPCR) was performed using Fast SYBR Green on a StepOnePlus system (Applied Biosystems). The following PCR primers were used: human β-actin: forward: 5′-TGGATCAGCAAGCAGGAGTATG-3′, reverse: 5′-GCATTTGCGGTGGACGAT-3′, human LDLR: forward: 5′-CCCGACCCCTACCCACTT-3′, reverse: 5′-AATAACACAAATGCCAAATGTACACA-3′, human PLK3: forward: 5′-CTGCGCCATGACTTCTTTACC-3′, reverse: 5′-GTCACGCAGCTGCTGATAGG-3′, human VEGFA: forward: 5′-CGAGGGCCTGGAGTGTGT-3′, reverse: 5′-CCGCATAATCTGCATGGTGAT-3′, Red Fluorescent Protein (RFP): forward: 5′-AGACCACCTACATGGCCAAGA-3′, reverse: 5′-CTCGTTGTGGGAGGTGATGTC-3′, Luc2: forward: 5′-ACGAGCACTTCTTCATCGTG-3′, reverse: 5′-CCTGGTAGCCCTTGTATTTGA-3′.

Half-lives of mRNAs were calculated by fitting an exponential decay curve to the mRNA levels determined at all time points.

Expression constructs

3′-UTR regions of LDLR mRNA were cloned into pDEST12.2 (Invitrogen), which contains a 5′-RFP tag. 3′-UTR regions of β-actin mRNA were cloned into pDEST12.2 (Invitrogen), which contains a 5′-LUC2 tag. Human ZFP36, ZFP36L1 and ZFP36L2 open reading frames were cloned into pDEST12.2 (Invitrogen), which

contains a 5′-MYC tag or a 5′-Flag tag, or into pDEST15 (Invitrogen).

Antibodies

The following antibodies were used for IP and/or western blot analysis: anti-β-actin (#4970; Cell Signalling), anti-CDK9 (sc-13130; Santa Cruz), anti-CNOT1 (14276-1-AP; Protein Tech), anti-CNOT7 (H00029883; Abnova), anti-FLAG (M2; Sigma), anti-hnRNPD (Q14103; Millipore), anti-HA (1867423; Roche), anti-IGF2BP1 (sc-21026; Santa Cruz), anti-KHSRP (ab83291; Abcam), anti-LARP7 (LaRP7-101AP; FabGennix Inc.), anti-LDLR (AF2148; BD Biosciences), anti-Myc (9E10; Roche), anti-phospho-ERK (#9101s; Cell Signalling), anti-phospho-MAPKAPK2 (#3007s; Cell Signalling), anti-phospho-RSK (sc-17033; Santa Cruz), anti-ZFP36L1 (#2119; Cell Signalling), anti-phospho-S6 (#2211; Cell Signalling).

Chemicals

Cells were treated with each chemical as described below. PMA (Sigma) was used at a final concentration of 100 ng/ml. U0126 (Cell Signalling) was used at a final concentration of 10 μM. BI-D1870 (Stemgent) was used at a final concentration of 20 μM. SL0101 (Millipore) was used at a final concentration of 75 μM. Actinomycin D (ActD) (Calbiochem) was used at a final concentration of 5 μg/ml.

Isobaric tags for relative and absolute quantitation (iTRAQ)-based quantification of phosphopeptides

FLAG-tagged ZFP36L1 and ZFP36L2 were transiently expressed in 293T cells. These proteins were purified using anti-Flag (M2) agarose beads (Sigma) and subjected to in solution digestion by lysyl endopeptidase and trypsin. Digested peptide mixtures were labeled with iTRAQ reagents (114 for PMA-treated sample; 115 for PMA+U0126-treated sample; 116 for untreated sample) according to the manufacturer's instructions and then loaded onto Fe-charged Probond (Fe-IMAC) columns (Applied Biosystems) (12). Loading/washing buffer for Fe-IMAC columns was 0.1% trifluoroacetic acid, 60% acetonitrile. After washing, bound peptides were eluted with 1% phosphate. Peptides were analyzed using a nanoLC/MS/MS system (QSTAR Elite, AB/MDS-Sciex) and a nanoLC system (Paradigm MS2, Michrom BioResources). Peak lists were obtained from the script using Analyst QS 2.0. MASCOT searches were performed against IPI human ver.3.1.6.

Short interfering RNA and antisense oligonucleotides

Short interfering RNAs (siRNAs) against human ZFP36L1 (Cat. No. HSS101104, HSS101101) and ZFP36L2 (Cat. No. HSS101105, HSS101102) and control siRNA (Cat. No. 12935-100) were purchased from Invitrogen. These siRNAs were transfected into cells using DarmaFECT 2 (Thermo Scientific) at a final concentration of 20 nM. All the antisense-oligonucleotides against human LDLR mRNA were fully LNA-modified and were purchased from Gene Design Inc.: Oligo-L1 (5′-AGATGAATAAA-3′), Oligo-L2 (5′-GCCTCCCAGAT-3′), Oligo-L3 (5′-CACTTAATAAA-3′), Oligo-L4 (5′-ATAATAACACA-3′), Oligo-L5 (5′-AGATGAAGAAA-3′), Oligo-L6 (5′-AGAATAATAGA-3′). These oligonucleotides were transfected into cells using DarmaFECT 2 (Thermo Scientific) at a final concentration of 80 nM.

Analysis of direct phosphorylation

Wild-type and mutant GST-ZFP36L1 were expressed in *Escherichia coli* and purified using glutathione-sepharose (GE). Two micrograms of purified GST-ZFP36L1 (unedited from glutathione-sepharose beads) and 0.5 μg of purified kinase were incubated in a kinase assay buffer [25 mM Tris (pH 7.5), 10 mM $MgCl_2$, 2 mM Na_3VO_4, 1 mM dithiothreitol (DTT), 1 mM adenosine triphosphate] at 30°C for 30 min with continuous mixing (total volume of 100 μl). Glutathione-sepharose beads were washed in wash buffer [10 mM HEPES (pH 7.5), 150 mM NaCl, 0.1% Triton X-100] three times. We then analyzed the phosphorylation of GST-ZFP36L1 using MS. We also examined the ability of GST-ZFP36L1 proteins to interact with CNOT using IP and western blot analysis.

Cell-based DiI-LDL uptake assay

Hep3B cells were transfected with indicated oligos. Twenty-four hours after transfection, cells were treated with DiI-LDL (final concentration 1 μg/ml, Molecular Probes) for 1 h and then lysed in RIPA buffer (25 mM Tris–HCl pH 7.6, 150 mM NaCl, 1% NP-40, 1% sodium deoxycholate, 0.1% SDS). DiI-LDL fluorescence (excitation/emission at 530/590 nm) was read on an Infinite 200 (Tecan) and protein levels were quantified using a BCA Protein Assay Kit (Thermo). For data analysis, the ratio of DiI-LDL fluorescence/protein concentration was used to normalize DiI-LDL uptake into cells.

RESULTS

To identify the critical protein controlling the stability of LDLR mRNA, we first developed the method of Flag-peptide-tagging the 3′-end of *in vitro* transcribed RNA (Supplementary Figure S1A and B; see Experimental Procedures). We then validated whether Flag-peptide-tagged RNA can be used to co-immunoprecipitate its binding protein, using HA-tagged-MS2 and a Flag-peptide-tagged-RNA that contains an MS2-binding site (13) (Supplementary Figure S1C). We found that Flag-peptide-tagged RNA can be used for co-immunoprecipitation of its binding protein (Supplementary Figure S1D). Next, we hypothesized that the critical protein controlling LDLR mRNA stability would bind specifically to its 3′-UTR region, but would not bind to stable mRNAs or unstable mRNAs that are not stabilized by PMA treatment. We then selected seven bait RNAs, including LDLR mRNA, five stable RNAs (β-actin mRNA, IFNA1 mRNA, MBP mRNA, hnRNP A2/B1 mRNAs and 7SK RNA) and one very unstable mRNA, c-Myc, which is not stabilized by PMA treatment (Table S1). We synthesized these RNAs *in vitro* and conjugated a

Flag-peptide to their 3′-ends. We performed an IP experiment using these seven bait RNAs and a 293T cell lysate. The co-immunoprecipitated proteins were eluted using the Flag peptide, and then digested with lysyl endopeptidase, and all peptides obtained were directly analyzed by MS (Figure 1A). For each RNA, we conducted two independent IP experiments and performed MS analysis in duplicate to obtain four sets of data. We identified about 400 kinds of peptides derived from ~150 proteins (Table S2). Approximately 25% of these proteins, including IGF2BP1, were common to all the RNA baits. We then extracted the LDLR mRNA-specific binding proteins that were only identified in all four MS analyses of LDLR samples and found ZFP36L1 and ZFP36L2 as proteins that bind specifically to the LDLR mRNA 3′-UTR (ARE1–3) (Table S3). Using this method, we also found well-known 7SK RBPs, including CDK9 and LARP7 as 7SK-Flag specific binding porteins (14) (Table S4). This result demonstrates the accuracy of our strategy. We confirmed the interactions of bait RNAs and their specific binding proteins by western blotting (Figure 1B). To further confirm the endogenous interaction between LDLR mRNA and ZFP36L1, we performed a co-immunoprecipitation experiment using the antibody against ZFP36L1 and 293T cell lysate. We found that endogenous ZFP36L1 interacts with LDLR mRNA, and also with PLK3 and VEGFA mRNAs, previously identified ZFP36L1-interacting mRNAs (7,8). ZFP36L1 did not interact with β-actin mRNA (Figure 1C).

ZFP36L1 and ZFP36L2 bind to LDLR mRNA

ZFP36L1 and ZFP36L2 are known as proteins that bind to a certain type of ARE that contains the sequence UAUUUAUU, causing destabilization of target mRNAs. The LDLR mRNA 3′-UTR contains three AREs (ARE1–3) (4); ARE1 and ARE2 are comprised of the UAUUUAUU sequence. We investigated the region responsible for LDLR mRNA instability and PMA-mediated stabilization (PMA is an activator of ERK) in an ActD chase experiment. After transfection of 293T cells with the reporter constructs, RFP-LDLR-3′-UTR-ARE1–3, RFP-LDLR-3′-UTR-ARE2–3 or RFP-LDLR-3′-UTR-ARE1, we examined the stability of the reporter mRNA and the effect of PMA on stability using quantitative reverse-transcription (RT)-PCR (qPCR) analysis. We also calculated the half-life of each RFP-reporter mRNA (Figure 2A and B). We found that the ARE1-containing region is not only responsible for LDLR mRNA instability, but is also responsible for PMA-mediated stabilization of LDLR mRNA.

We then investigated which regions of the LDLR mRNA 3′-UTR are responsible for binding to ZFP36L1 and ZFP36L2 using several Flag-peptide-tagged 3′-UTR fragments of the LDLR mRNA, including LDLR-3′-UTR-ARE1–3, LDLR-3′-UTR-ARE2–3 and LDLR-3′-UTR-ARE1. We found that ZFP36L1 and ZFP36L2 predominantly bind to the ARE1 region, and only modestly bind to the ARE2–3 region, despite the presence of the UAUUUAUU sequence (Figure 2A and C).

To confirm the binding of ZFP36L1 and ZFP36L2 to the UAUUUAUU sequence of ARE1, we used LNA-modified antisense oligonucleotides. First, we designed LNA-modified 11-base oligonucleotides (Oligo-L1–L4). Oligo-L1 was complementary to the evolutionary conserved UAUUUAUU sequence in the ARE1 region, and to an LDLR gene-specific sequence located immediately 3′ to the UAUUUAUU sequence (Figure 2A and Supplementary Figure S2A). Oligo-L2 was designed to interact with the 3′-flanking region of the UAUUUAUU sequence, but not with UAUUUAUU itself (Figure 2A). Oligo-L3 and -L4 were designed to be complementary to the LDLR mRNA ARE-2 and -3 regions, respectively (Figure 2A). We then performed co-immunoprecipitation experiments with or without Oligo-L1, -L2, -L3 and -L4 to examine the ability of oligonucleotides to disrupt the *in vitro* interaction between LDLR mRNA and ZFP36L1 or ZFP36L2. We found that interaction was clearly blocked by Oligo-L1, but was not affected by Oligo-L2, -L3 or -L4 (Figure 2D). On the other hand, Oligo-L1 did not disrupt the interaction between LDLR mRNA and KHSRP, hnRNPD or hnRNPI, which have recently been identified as LDLR mRNA-destabilizing proteins (Supplementary Figure S2B). Furthermore, Oligo-L1 had no effect on the interaction between ZFP36L1 and the 3′-UTR regions of VEGFA or PLK3 mRNAs, recently identified as target mRNAs of ZFP36L1 (7,8), (Supplementary Figure S2B). These results indicate that ZFP36L1 and ZFP36L2 predominantly interact with the UAUUUAUU sequence of the ARE1 region of the LDLR mRNA 3′-UTR.

ZFP36L1 and ZFP36L2 destabilize LDLR mRNA

To investigate the significance of the interaction between LDLR mRNA and ZFP36L1 or ZFP36L2, we performed double siRNA-mediated knockdown of ZFP36L1 and ZFP36L2. We used HeLa cells because siRNA-mediated gene silencing is more efficient in HeLa cells than in HEK293T cells (15). We first examined the efficiency of knockdown using qPCR (Supplementary Figure S3A). We then examined the effect of this knockdown on LDLR mRNA and protein levels. We found that knockdown of ZFP36L1 and ZFP36L2 together resulted in an increase in both LDLR mRNA and protein (Figure 3A and B, Supplementary Figure S3B). Next, we examined the effect of siRNA on LDLR mRNA stability using an ActD chase experiment. We found that LDLR mRNA in cells transfected with ZFP36L1 and ZFP36L2 siRNA was clearly more stabilized than that in control siRNA-transfected cells (Figure 3C, Supplementary Figure S3C). We also observed PMA-mediated LDLR mRNA stabilization in cells transfected with control siRNA but, interestingly, not in cells transfected with ZFP36L1 and ZFP36L2 siRNAs (Figure 3C, Supplementary Figure S3C). These results suggest that ZFP36L1 and ZFP36L2 are LDLR mRNA-destabilizing factors that are indispensable for PMA-mediated stabilization of LDLR mRNA. ZFP36L1 and ZFP36L2-mediated LDLR mRNA destabilization was also observed in other cell lines, including 293T cells and Hep3B cells, indicating that this regulation is conserved among these cells (Supplementary Figure S3D).

To further confirm that the ZFP36L1 and ZFP36L2-mediated destabilization of LDLR mRNA is caused by di-

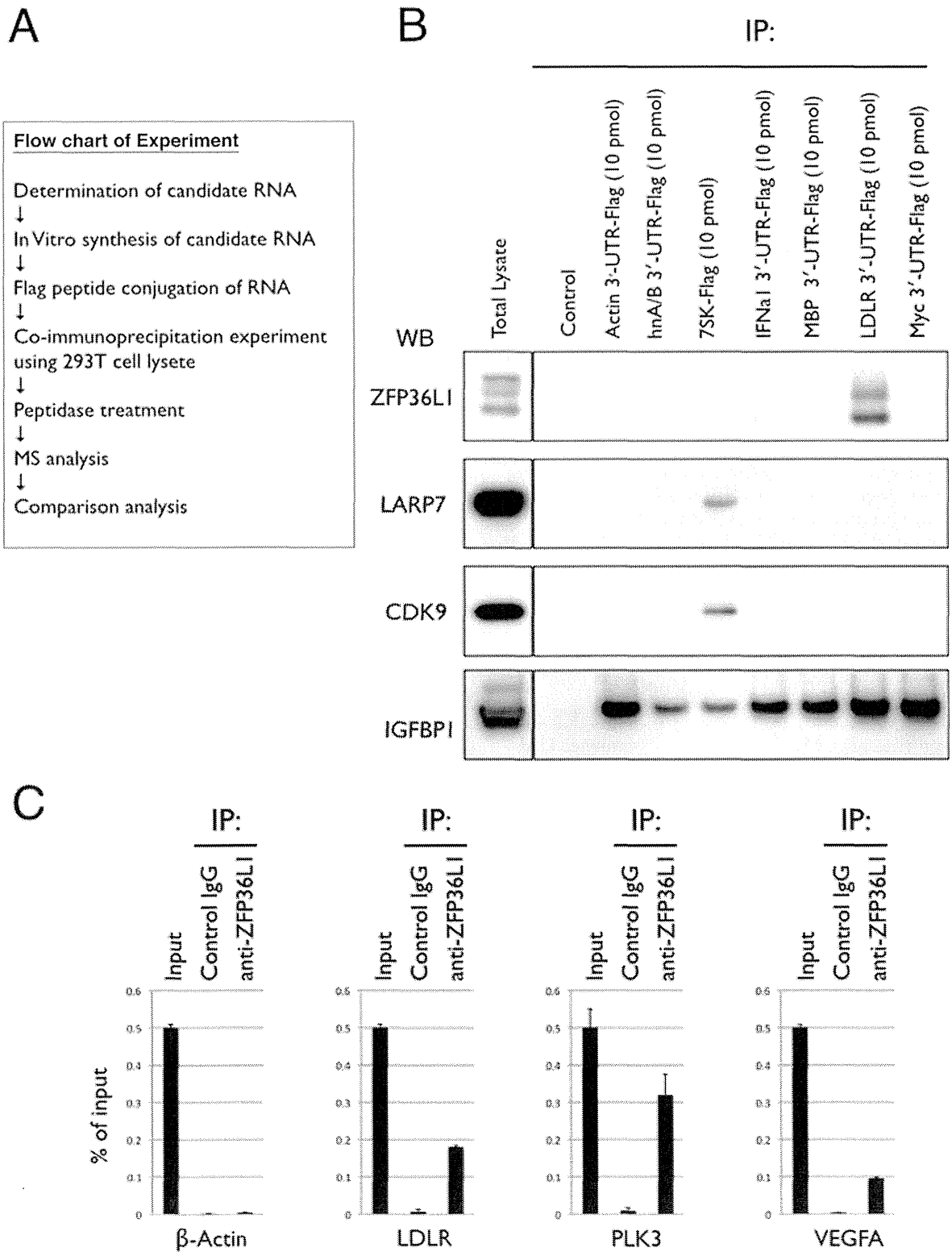

Figure 1. Identification of bait-specific RBPs. (**A**) Flow chart summarizing the experiment. (**B**) Confirmation of our results by western blot analysis. 293T cells were lysed in lysis buffer and the cleared lysates were subjected to IP with anti-Flag antibody in combination with the indicated bait RNAs. Co-immunoprecipitated RNA and proteins were eluted using the Flag-peptide and were then subjected to western blot analysis using the indicated antibodies. Five percent of the initial amount of cleared 293T lysate was loaded as total lysate. An IP experiment without bait RNA was performed as a control. (**C**) Confirmation of the endogenous interaction between ZFP36L1 and LDLR mRNA. 293T cells were lysed in lysis buffer and the cleared lysates were subjected to IP with control or anti-ZFP36L1 antibody. Total RNA and co-immunoprecipitated RNA were extracted, and quantitative reverse-transcription (RT)-PCR (qPCR) was performed using primers specific to LDLR, PLK3, VEGFA and β-actin mRNAs. Results are shown as% of input. The data are representative of at least three independent experiments. Error bars show standard deviation of the mean.

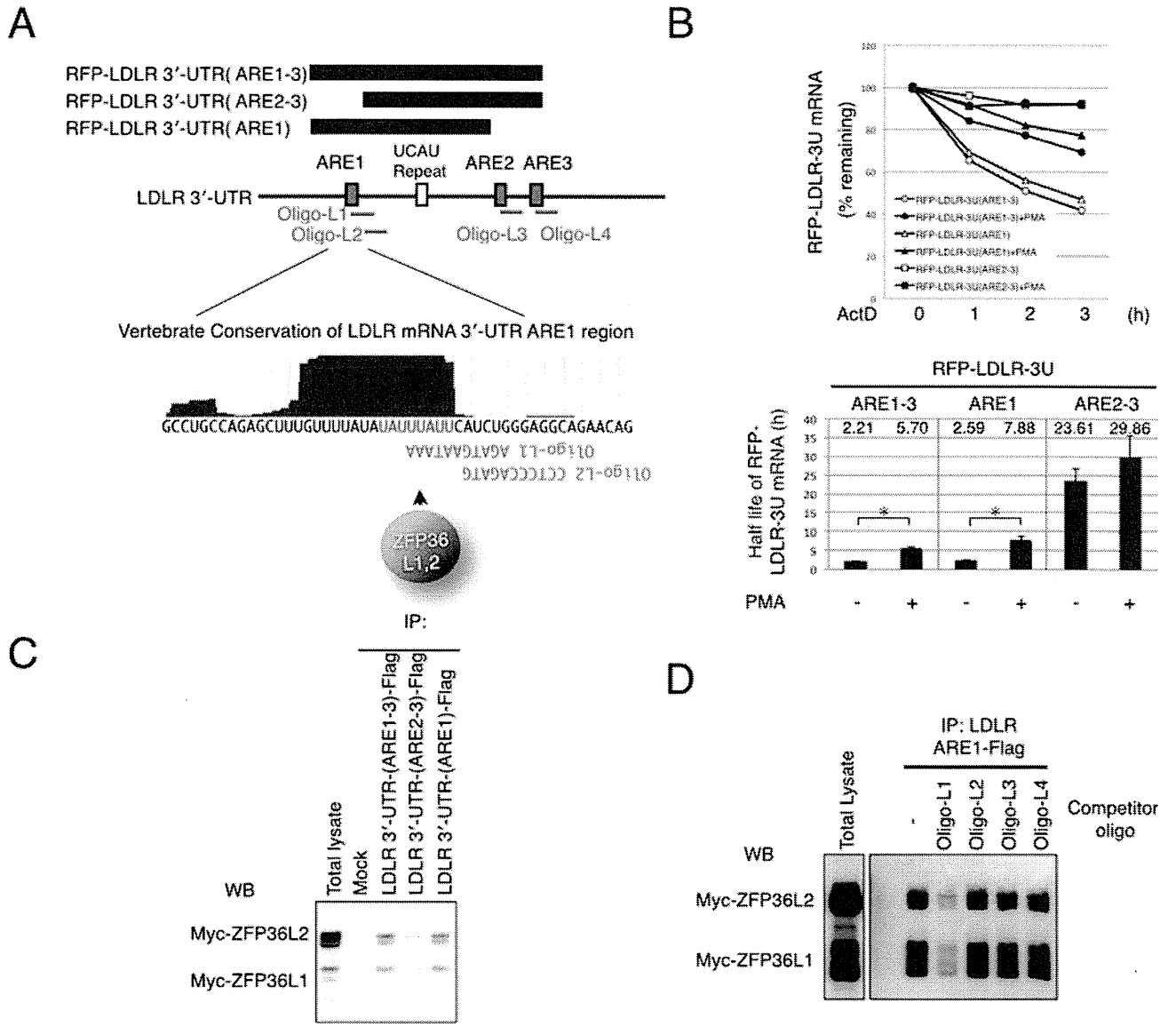

Figure 2. Domain analysis of the 3′-UTR of LDLR mRNA. (**A**) Schematic representation of the 3′-UTR of LDLR mRNA. Black bars indicate the regions used for ActD chase and IP experiments. AREs 1–3 are indicated by red boxes and the UCAU repeat is indicated by the white box. Designed oligonucleotides are indicated by blue lines. Conservation around the LDLR ARE1 region is shown in the blue graph, created using Vertebrate Multiz Alignment & PhastCons Conservation (28 species), as extracted from the UCSC Human Genome Browser (http://genome.ucsc.edu/). The consensus ZFP36L1- and ZFP36L2-binding sequence is colored in red. Sequences of the designed oligonucleotides, L1 and L2, are indicated. (**B**) RFP-tagged LDLR 3′-UTR constructs were expressed in 293T cells, and cells were then subjected to ActD chase experiments. Twenty-four hours after transfection, 293T cells were treated with ActD and PMA as indicated (PMA treatment commenced 10 min after ActD treatment). qPCR was performed using RFP and Luc2-specific primers. Results were normalized to the levels of Luc2 mRNA. The data are representative of at least three independent experiments. mRNA half-lives were calculated by fitting an exponential decay curve to all time points. Figures in the graph indicate the mean value of the mRNA decay half-lives. Error bars show standard deviation of the mean. *P*-values were calculated using Student's *t*-test. $*P < 0.002$; $n = 3$ for each group. (**C**) 293T cells were transfected with Myc-tagged ZFP36L1 and ZFP36L2. Cells were then lysed with lysis buffer and the cleared lysates were subjected to IP with the indicated LDLR 3′-UTR bait RNAs. Immunoprecipitated proteins were subjected to western blot analysis with the anti-Myc antibody. (**D**) 293T cells were transfected with Myc-tagged ZFP36L1 and ZFP36L2. Cells were then lysed with lysis buffer and the cleared lysates were subjected to IP with the indicated LDLR 3′-UTR bait RNAs and the indicated oligos. Immunoprecipitated proteins were subjected to western blot analysis with the anti-Myc antibody. These data are representative of at least three independent experiments.

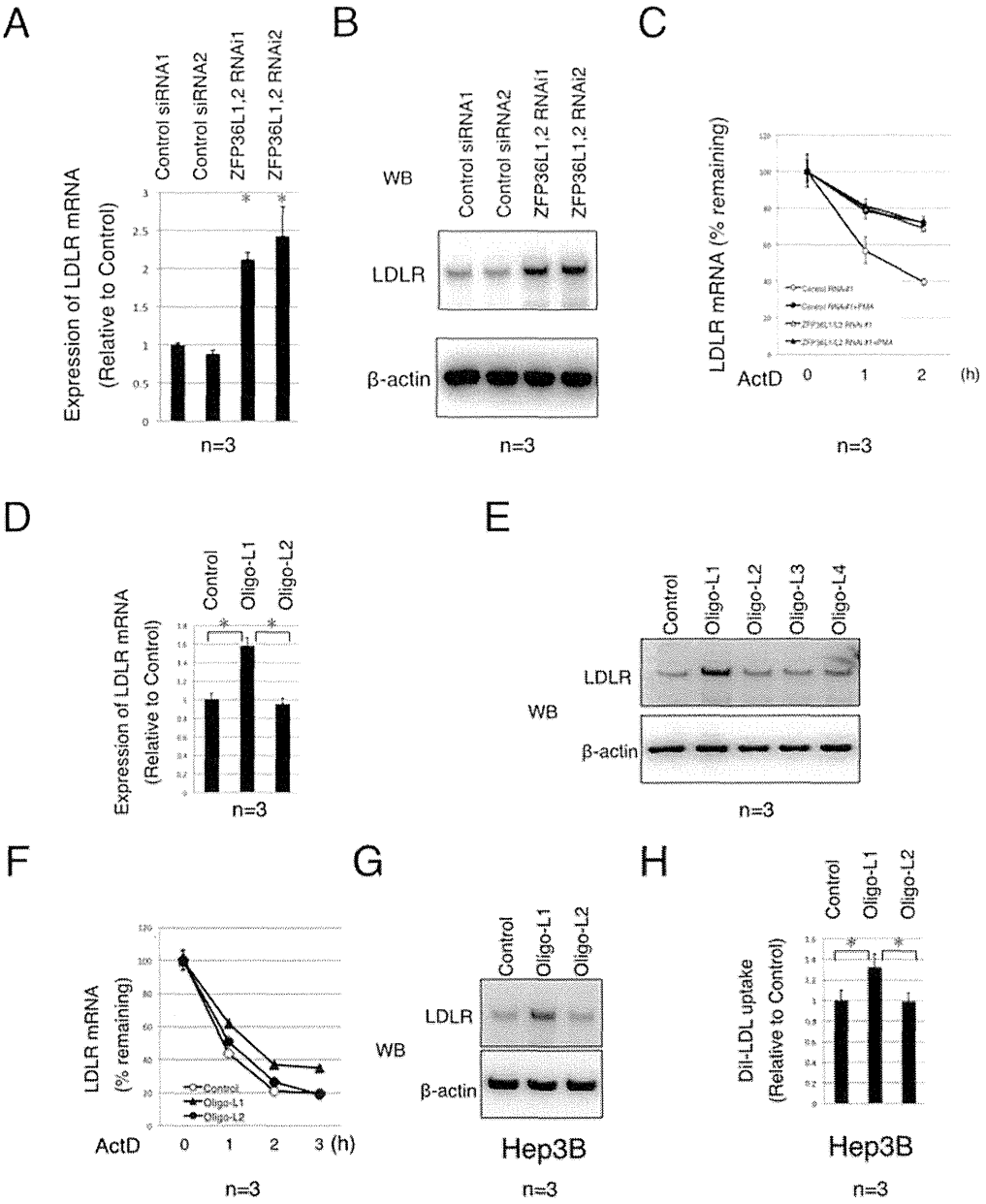

Figure 3. LDLR mRNA is destabilized by ZFP36L1 and ZFP36L2. (**A**) HeLa cells were transfected with ZFP36L1 and ZFP36L2 siRNAs. Forty-eight hours after transfection, cells were harvested, total RNA was extracted and quantitative RT-PCR (qPCR) was performed using primers specific to LDLR mRNA and β-actin mRNA. Results were normalized to β-actin mRNA levels. Error bars show standard deviation of the mean. *P*-values against control were calculated using Student's *t*-test.*$P < 0.002$; $n = 3$ for each group. (**B**) Forty-eight hours after transfection, cells were harvested and the lysates were subjected to western blot analysis using the indicated antibodies. (**C**) Forty-eight hours after transfection, cells were treated with ActD and chased for the indicated time with or without PMA (PMA treatment commenced 10 min after ActD treatment). Total RNA was extracted and qPCR was performed using primers specific to LDLR mRNA and β-actin mRNA. Results were normalized to the levels of β-actin mRNA. Error bars show standard deviation of the mean. (**D**) HeLa cells were transfected with the indicated oligos. Twenty-four hours after transfection, cells were harvested and total RNA was extracted. Quantitative RT-PCR (qPCR) was performed using primers specific for LDLR and β-actin. Results were normalized to β-actin mRNA levels. Error bars show standard deviation of the mean. *P*-values against control were calculated using Student's *t*-test. *$P < 0.002$; $n = 3$ for each group. (**E**) HeLa cells were transfected with the indicated oligos. Twenty-four hours after transfection, cells were harvested and the lysates were subjected to western blot analysis using the indicated antibodies. (**F**) HeLa cells were transfected with the indicated oligos. Twenty-four hours after transfection, cells were treated with ActD and chased for the indicated times. Total RNA was extracted and qPCR was performed using primers specific to LDLR mRNA and β-actin mRNA. Results were normalized to the levels of β-actin mRNA. Error bars show standard deviation of the mean. (**G**) Hep3B cells were transfected with the indicated oligos. Twenty-four hours after transfection, cells were harvested and the lysates were subjected to western blot analysis using the indicated antibodies. (**H**) Hep3B cells were transfected with the indicated oligos. Twenty-four hours after transfection, cells were treated with DiI-LDL for 1 h. The cells were then lysed in RIPA buffer and the ratio of DiI-LDL fluorescence/protein concentration was measured. Error bars show standard deviation of the mean. *P*-values against control were calculated using Student's *t*-test. *$P < 0.002$; $n = 3$ for each group. The data are representative of at least three independent experiments. The number below the figure indicates the number of times we replicated the experiment. Data from one of the independent experiments are shown in Supplementary Figure S4A–H.

rect interaction, we examined the effect of LNA-modified oligonucleotides (as used in the experiment presented in Figure 2D) on the levels of LDLR mRNA and LDLR protein. We transfected these oligonucleotides into HeLa cells and found that Oligo-L1 increased the levels of LDLR mRNA and protein (Figure 3D and E, Supplementary Figure S3E). In contrast, Oligo-L2, -L3 and -L4 had no effect on the levels of LDLR mRNA or protein (Figure 3D and E, Supplementary Figure S3E). In addition, as expected, Oligo-L1 had no effect on the levels of VEGFA or PLK3 mRNAs (Supplementary Figure S3F). We also examined the effect of Oligo-L1 on the stability of LDLR mRNA in HeLa and 293T cells using an ActD chase experiment and we found that Oligo-L1 stabilized LDLR mRNA in these cell lines (Figure 3F, Supplementary Figure S3G and H). We then used two further oligonucleotides, Oligo-L5 and Oligo-L6. Oligo-L5 is a point mutant of Oligo-L1 (T8G) and Oligo-L6 is a scrambled oligonucleotide of Oligo-L1. Neither of these oligonucleotides could inhibit the interaction between LDLR mRNA and ZFP36L1, nor could they increase the stability of LDLR mRNA or the levels of LDLR protein in cells (Supplementary Figure S3I and J)

We finally used human liver-derived Hep3B cells, because we anticipate that this approach could potentially increase the levels of LDLR protein in the liver, thereby lowering blood LDL cholesterol levels. We transfected Oligo-L1 and Oligo-L2 into Hep3B cells and again found that Oligo-L1 stabilized LDLR mRNA and increased the levels of LDLR protein (Figure 3G, Supplementary Figure S3K and L). We then examined the effect of these oligonucleotides on LDL incorporation in Hep3B cells using DiI-labeled LDL. As expected, we found that Oligo-L1 increased LDL incorporation into Hep3B cells (Figure 3H). These results indicate that, LNA-modified antisense oligonucleotides can increase the LDL-uptake activity of liver-derived cells.

ZFP36L1 is regulated by phosphorylation downstream of ERK

Next, we investigated the underlying mechanisms of PMA-ERK-mediated LDLR mRNA stabilization. Given that ERK is a critical kinase in PMA-mediated LDLR mRNA stabilization (4), we examined whether ZFP36L1 is phosphorylated downstream of ERK. We found that PMA treatment induced an electrophoretic mobility shift of ZFP36L1, which could be reversed when cells were treated with PMA and U0126, a specific inhibitor of the ERK pathway (Figure 4A). We also found that the mobility shift of Flag-ZFP36L1, which we immunopurified from Flag-ZFP36L1-overexpressing and PMA-treated 293T cells, could be reversed by treatment with bacterial alkaline phosphatase (Figure 4B). These results indicate that ZFP36L1 is phosphorylated downstream of ERK. We then analyzed the ERK-dependent phosphorylation sites using an iTRAQ-based quantitative MS approach. We immunopurified Flag-ZFP36L1 protein from mock-, PMA- or PMA + U0126-treated 293T cells and determined the ERK-dependent phosphorylation sites. We found that phosphorylation of the C-terminal serine-334 residue of ZFP36L1 and of the C-terminal serine-493 and -495 residues of ZFP36L2 was increased upon PMA treatment, but was reversed by U0126 treatment (Figure 4C, Supplementary Figure S5A). This result indicates that the phosphorylation of these residues is ERK -dependent. We also analyzed the phosphorylation of endogenous ZFP36L1, which we purified from 293T cell lysate using a Flag-tagged LDLR ARE1 region (Supplementary Table S1), and found that the C-terminal serine-334 residue of endogenous ZFP36L1 is also phosphorylated upon PMA treatment (Supplementary Figure S5B and C).

To understand the function of ZFP36L1 phosphorylation, we first examined whether PMA treatment decreases the RNA-binding ability of ZFP36L1 and ZFP36L2. We found that PMA treatment slightly increased the interaction between Myc-ZFP36L1 and LDLR mRNA, while that with Myc-ZFP36L2 was not affected by PMA treatment (Figure 4C). We found that the RNA-binding ability of endogenous ZFP36L1 was also slightly increased by PMA treatment (Supplementary Figure S5B). These results indicate that PMA treatment does not inhibit the RNA-binding ability of ZFP36L1 and ZFP36L2.

The CCR4-NOT deadenylase complex has recently been shown to interact with the C-terminus of ZFP36 (16,17); therefore, we next examined whether ZFP36L1 interacts with the CCR4-NOT deadenylase complex and whether this interaction is affected by PMA. We found that CNOT7, a critical enzymatic component of CCR4-NOT deadenylase, interacts with ZFP36L1 and interestingly, this interaction is inhibited by PMA treatment and reversed by U0126 treatment, indicating that this regulation is mediated by the ERK pathway (Figure 4E). To confirm that this effect was due to C-terminal phosphorylation, we constructed the ZFP36L1-ΔC mutant (in which C-terminal amino acid residues, including all conserved phosphorylation sites, were deleted) and the ZFP36L1-SASA mutant (in which serine-334 and -336 were mutated to alanine residues, mimicking constitutive de-phosphorylation) (Figure 4F). We then examined the interaction between CNOT7 and these ZFP36L1 mutants and found that the ZFP36L1-SASA mutant retained the ability to interact with CNOT7 after PMA treatment, whereas the ZFP36L1-ΔC mutant did not (Figure 4G). Surprisingly, we also found that PMA treatment still caused an electrophoretic mobility shift of the ZFP36L1-SASA mutant. These results indicate that the interaction between ZFP36L1 and CNOT7 is regulated by ERK-mediated C-terminal phosphorylation of ZFP36L1. Furthermore, C-terminal phosphorylation of ZFP36L1 is not responsible for the PMA-mediated electrophoretic mobility shift.

We considered the possibility that ZFP36 and ZFP36L2 could also be regulated by PMA because the C-terminal region is highly conserved in members of the ZFP36 protein family (Figure 4C). We examined the interaction between CNOT7 and ZFP36 or ZFP36L2 and found that ZFP36L2, in addition to ZFP36 and ZFP36L1, also interacts with CNOT7 and that the interactions between CNOT7 and ZFP36 or ZFP36L2 are inhibited by PMA treatment (Supplementary Figure S5E). Thus, ERK-mediated regulation may be conserved among members of the ZFP36 family.

We further validated the function of ZFP36L1 phosphorylation in LDLR mRNA-destabilization. We transfected the RFP-LDLR-3′-UTR expression vector and a luciferase-β-actin-3′-UTR vector along with ZFP36L1-